

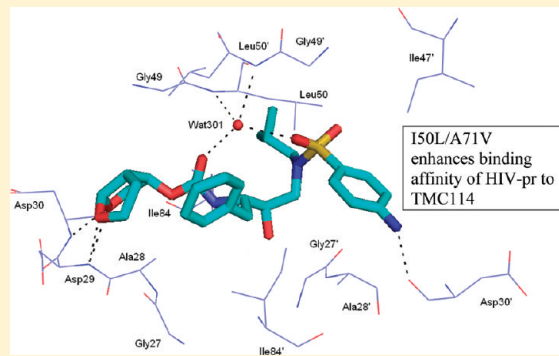
Interaction of I50V Mutant and I50L/A71V Double Mutant HIV-Protease with Inhibitor TMC114 (Darunavir): Molecular Dynamics Simulation and Binding Free Energy Studies

Biswa Ranjan Meher and Yixuan Wang*

Computational Chemistry Laboratory, Department of Natural Sciences, Albany State University, Albany, Georgia 31705, United States

Supporting Information

ABSTRACT: In the present work, the binding of inhibitor TMC114 (darunavir) to wild-type (WT), single (I50V) as well as double (I50L/A71V) mutant HIV-proteases (HIV-pr) was investigated with all-atom molecular dynamics (MD) simulations as well as molecular mechanics-Poisson-Boltzmann surface area (MM-PBSA) calculation. For both the apo and complexed HIV-pr, many intriguing effects due to double mutant, I50L/A71V, are observed. For example, the flap–flap distance and the distance from the active site to the flap residues in the apo I50L/A71V–HIV-pr are smaller than those of WT- and I50V–HIV-pr, probably making the active site smaller in volume and closer movement of flaps. For the complexed HIV-pr with TMC114, the double mutant I50L/A71V shows a less curling of the flap tips and less flexibility than WT and the single mutant I50V. As for the other previous studies, the present results also show that the single mutant I50V decreases the binding affinity of I50V–HIV-pr to TMC, resulting in a drug resistance; whereas the double mutant I50L/A71V increases the binding affinity, and as a result of the stronger binding, the I50L/A71V may be well adapted by the TMC114. The energy decomposition analysis suggests that the increase of the binding for the double mutant I50L/A71V–HIV-pr can be mainly attributed to the increase in electrostatic energy by -5.52 kcal/mol and van der Waals by -0.42 kcal/mol , which are canceled out in part by the increase of polar solvation energy of 1.99 kcal/mol . The I50L/A71V mutant directly increases the binding affinity by approximately -0.88 (Ile50 to Leu50) and -0.90 (Ile50' to Leu50') kcal/mol, accounting 45% for the total gain of the binding affinity. Besides the direct effects from the residues Leu50 and Leu50', the residue Gly49' increases the binding affinity of I50L/A71V–HIV-pr to the inhibitor by -0.74 kcal/mol , to which the electrostatic interaction of Leu50's backbone contributes by -1.23 kcal/mol . Another two residues Ile84 and Ile47' also increase the binding affinity by -0.22 and -0.29 kcal/mol , respectively, which can be mainly attributed to van der Waals terms ($\Delta T_{\text{vdw}} = -0.21$ and -0.39 kcal/mol).



1. INTRODUCTION

Protease inhibitors (PIs) play a very important role in combating AIDS through deactivating HIV-1 protease (HIV-pr, shown in Figure 1) that acts at the late stage of infection by cleaving the Gag and Gag–Pol polyproteins to yield mature infectious virions.¹ However, their effectiveness were greatly affected by variant mutations of the HIV-pr. Mutations causing drug resistance have been therefore one of the biggest challenges for the treatment of HIV replication.² TMC114, a nonpeptidic compound terminated by the bis-tetrahydrofuran (bis-THF) moiety shown in Figure 2, is an extremely potent PI for treatment of drug resistant HIV strains including many subtypes.³ It is speculated that the bis-THF oxygen atoms may form hydrogen bonds with the backbone N–H groups of residues Asp30 (Asp30') of HIV-pr, enhancing the binding of the PI with HIV-pr.³ As for other approved PIs, several HIV-pr mutants were demonstrated to have drug resistance over the TMC114, like D30N and I50V, whereas L90M is well adapted by the TMC114.^{4,5} The drug resistance mechanism of such

mutants was explored at the molecular level with all-atomistic MD simulation combined with molecular mechanics-Poisson/Boltzmann surface area (MM-PBSA) for the binding energies of TMC114 to D30N and I50V mutants.⁶ It was found that loss of H-bonds between Asp30 and TMC114 drives the drug resistance in D30N, whereas for I50V, it is the increased polar solvation energies for the two residues Asp30' and Val50'.⁶ The resistance of the inhibitor GRL-98065, an analogue of TMC114 where just the aniline group is replaced by a 1,3-benzodioxole group, to mutants I50V and V82A was attributed to a higher entropic contribution than in the wild-type (WT) HIV-pr, and the reduced van der Waals may be responsible for the drug resistance of I84V to GRL-98065.⁶ There have been several other studies on ligand binding interactions and multidrug resistance in HIV-pr using the MM-PBSA method.^{7–13}

Received: August 4, 2011

Revised: January 11, 2012

Published: January 12, 2012

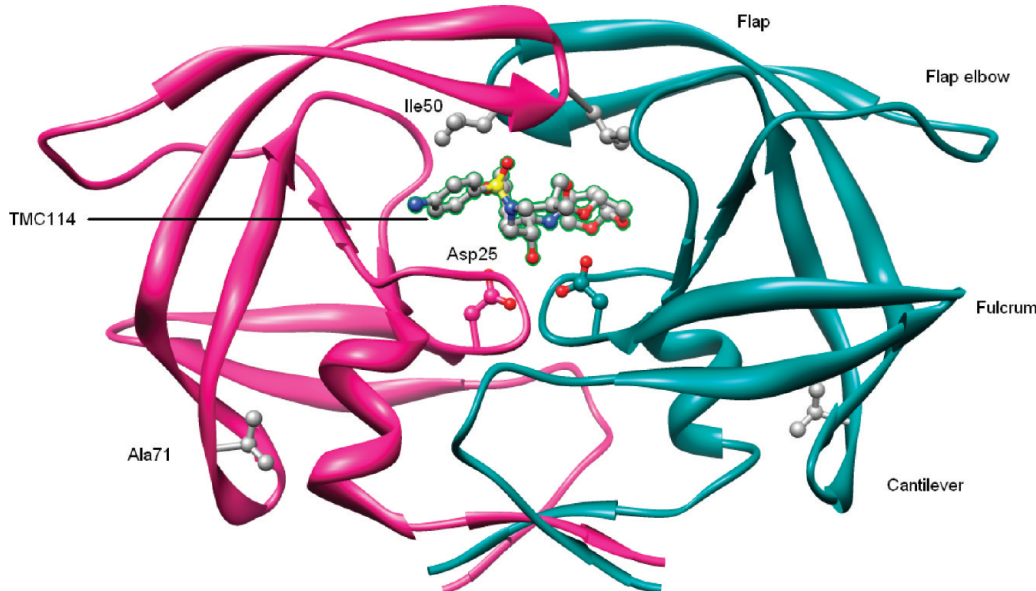


Figure 1. Structure of HIV-pr complexed with TMC114. The HIV-pr is shown in magenta and cyan ribbons for chain-A and chain-B, respectively. Catalytic residues (Asp25 and Asp25') and the sites of mutation (Ile50 and Ala71) are represented by ball and stick. TMC114 is bound in the active site and is labeled. Important regions of the HIV-pr like flap, flap elbow, fulcrum, and cantilever are also shown.

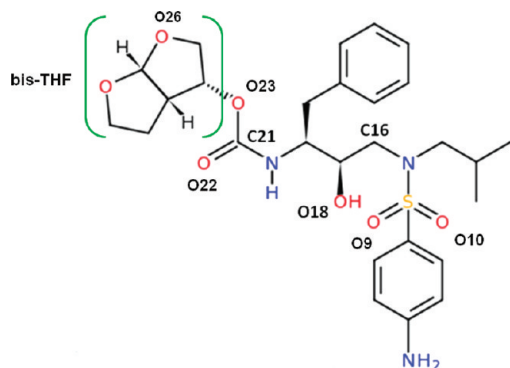


Figure 2. Molecular structure of the inhibitor TMC114. The moiety bis-THF is labeled with a square bracket in the color green. Important atoms like O9, O10, O18, and O22, which are involved in the interactions between the inhibitor and protein, are also labeled in black bold letters.

Mutation I50V and the double mutation I50L/A71V are considered as two of the most key residue mutations of the HIV-pr drug resistance to inhibitors in clinical use. However, although both of the residues are present in two critical locations and their effect on a few other PIs were previously discussed,¹⁴ for the double mutation I50L/A71V, there is little information regarding its importance in the drug resistance mechanism for the TMC114. Mutation I50L is a signature mutation for atazanavir (ATV) resistance and has increased susceptibility to other inhibitors with the presence of other primary and secondary resistance mutations.¹⁵ A71V mutation in the cantilever region is distant from the active site and has a profound effect on the binding of ligands to the active site through H-bond propagation from the site of mutation.¹⁶ With isothermal titration calorimetry, Yanchunas et al. showed that protease enzymes containing I50L/A71V exhibit increased binding to seven inhibitors relative to wild-type HIV-pr, being parallel to the increased susceptibility of recombinant viruses with this mutation.^{14,17} Thus, the double mutation (I50L/A71V)

effect of the two important residues Ile50 and Ala71 on HIV-pr structure and its difference from the single mutation (I50V) influence, prompt us to investigate the changes in binding affinity of the inhibitor TMC114 to the protease.

In the present study, to facilitate the investigation of drug resistance mechanism and to obtain information about the binding of TMC114 to the WT and mutant HIV-pr, MD simulations have been performed first for three inhibitor-free (apo) WT, I50V, and I50L/A71V HIV-proteases as well as the three inhibitor-bound HIV-proteases. The major objective for the MD simulation is to explore the similarity and distinction for the dynamic behaviors of the three apo and bound proteins. For both the apo and complexed HIV-pr, the analysis indicates many intriguing effects due to double mutant, I50L/A71V. The flap curling and opening events in I50L/A71V–HIV-pr are more stable than those of WT and I50V mutant. The average flap tip–active site, flap–flap distances, and curling behavior of the TriCa angles suggest a closer movement of flaps in the double mutant as compared to WT and I50V, probably making the active site volume smaller. The most distinct motion for the HIV-pr complex was the movement of the side chain of catalytic Asp25 about the inhibitor. There is a flip-flop of the interaction between the catalytic Asp25 OD1/OD2 atoms and O18 of TMC114, which may be due to the effect of the mutation A71V from the double mutant, where the change from Ala to Val modifies the H-bonding pattern between the four antiparallel β -sheets connecting the Asp25 site to Val71. The change in H-bonding pattern induces the rearrangement of β -sheets and finally affects the dynamics of Asp25 residues.

To quantitatively describe the influence of the double mutant, the MM-PBSA method was then used to calculate the absolute binding free energies,^{18–25} which were further decomposed to a per-residue basis.²⁶ The primary objectives for the binding energy calculation are to gain an insight into whether the double mutant I50L/A71V provides drug resistance to TMC114, and then to analyze the detailed interaction mechanism at a molecular level. As for the other previous studies, the present results also show that the single

mutant I50V decreases the binding affinity of I50V–HIV-pr to TMC, resulting in a drug resistance. It is interesting to note that the double mutant I50L/A71V increases the binding affinity, and as a result of the stronger binding, the I50L/A71V may be well adapted by the TMC114.

2. THEORETICAL METHODOLOGY

2.1. System Setups. The crystal structures of the WT and mutant HIV-pr complexed with TMC-114 were obtained from the Protein Data Bank (PDB). 1T3R²⁷ for the WT HIV-pr, 2F8G⁴ for the I50V mutant, and 3EM6²⁸ for the I50V/A71V double mutant HIV-pr. There are alternate conformations in 3EM6 and 2F8G: conformation A and B, owing to the inconspicuous electron density of few residues in the HIV-pr, only conformation A was selected for the starting model. The apo variants of WT and mutant proteases were obtained by deletion of the inhibitors from the active site. Because of the importance of the protonation of Asp25/Asp25' in the HIV-pr, the monoprotonated HIV-pr was considered, and a proton is added to the oxygen atom OD2 in Asp25' in chain B.^{29,30} Charges of TMC114 were calculated using the restrained electrostatic potential (RESP) procedure³¹ at the HF/6-31G* after minimizing the molecule at the AM1 semiempirical level.³² GAFF force field³³ parameters and the RESP partial charges are assigned using the Antechamber module in the AMBER10 package.³⁴ All missing hydrogen atoms were added using the LEaP module. The ff99SB³⁵ force field with TIP3P³⁶ water models was used for all the simulations. The system was solvated with the TIP3P waters in the truncated octahedron periodic box of size $89.2 \times 84.8 \times 96.3 \text{ \AA}^3$ containing more than 9000 water molecules. The box size was chosen according to the approximate shape of each complex. A cutoff of 10 Å was used along the three axes from any solute atoms of the system. An appropriate number of Cl⁻ counterions were added to neutralize the net positive charge on the system. A default cutoff of 8.0 Å in AMBER10 was used for Lennard-Jones interactions, and the long-range electrostatic interactions were calculated with the particle mesh ewald (PME) method.³⁷ Constant temperature and pressure conditions in the simulation were achieved by coupling the system to a Berendsen's thermostat and barostat.³⁸ The SHAKE³⁹ algorithm was used to constrain all bonds involving hydrogens.

2.2. Molecular Dynamics Simulations. Structures were optimized through Sybyl before the minimization to remove any bad contacts in the structure. The system was then minimized in four phases. In the first phase, the system was minimized giving restraints (30 kcal/mol/Å²) to all heavy atoms of protein and ligand for 10 000 steps with subsequent second phase minimization of the all backbone atoms and C_α atoms, respectively, for 10 000 steps each. Then, the system was heated to 300 K with a gap of 50 K over 10 ps with a 1 fs time step. In subsequent minimization of the third phase, the force constant was reduced by 10 kcal/mol/Å² in each step to reach the unrestrained structure in three steps of 10 000 steps each. Finally, the whole system was minimized again for 10 000 steps without any constraint at the NVT ensemble. The system was equilibrated at the NVT ensemble for 100 ps and then switched over to the NPT ensemble equilibrating without any restraints for another 120 ps. The convergence of energies, temperature, pressure, and global rmsd was used to verify the stability of the systems. All the apo and complexed trajectories were run for 20 ns. The time step for a MD production run was 1 fs. The 20 ns trajectories were used to calculate the average structure

for all the systems. All the six apo and complexed MD simulations were performed with AMBER10³⁴ at the Pittsburgh Supercomputing Center on the SGI Altix Cobalt system at NCSA, requesting sixteen 8-core nodes, and on local Dell HPCC machines. The simulation time is approximately 1200 CPU hours of a single-core processor.

2.3. MM-PBSA Calculations. The binding free energies were calculated using the MM-PBSA method implemented in AMBER10.³⁴ For each complex, a total number of 50 snapshots were taken from the last 2 ns on the MD trajectory with an interval of 40 ps. The MM-PBSA method and nmode module in Amber10 were applied to calculate the binding free energy of the inhibitor TMC114 to the protease. The MM-PBSA method can be summarized as

$$\Delta G_b = \Delta E_{MM} + \Delta G_{sol} - T\Delta S \quad (1)$$

where ΔG_b is the binding free energy in solution consisting of the molecular mechanics free energy (ΔE_{MM}) and the conformational entropy effect to binding ($-T\Delta S$) in the gas phase, and the solvation free energy (ΔG_{sol}). ΔE_{MM} can be expressed as

$$\Delta E_{MM} = \Delta E_{vdw} + \Delta E_{ele} \quad (2)$$

where ΔE_{vdw} and ΔE_{ele} correspond to the van der Waals and electrostatic interactions in gas phase, respectively. The solvation free energy (ΔG_{sol}) is further divided into two components:

$$\Delta G_{sol} = \Delta G_{pol} + \Delta G_{nonpol} \quad (3)$$

where ΔG_{pol} and ΔG_{nonpol} are the polar and nonpolar contributions to the solvation free energy, respectively. The ΔG_{sol} is calculated with the PBSA module of the AMBER10 suite of programs. In our calculation, the dielectric constant is set to 1.0 inside the solute and 80.0 for the solvent. The nonpolar contribution of the solvation free energy is calculated as a function of the solvent-accessible surface area (SAS), as follows:

$$\Delta G_{nonpol} = \gamma(\text{SAS}) + \beta \quad (4)$$

where, SAS was estimated using the MSMS program, with a solvent probe radius of 1.4 Å. The values of empirical constants γ and β were set to 0.00542 kcal/(molÅ²) and 0.92 kcal/mol, respectively.

The contributions of entropy ($T\Delta S$) to binding free energy arise from changes of the translational, rotational, and vibrational degrees of freedom, as follows:

$$\Delta S = \Delta S_{translational} + \Delta S_{rotational} + \Delta S_{vibrational} \quad (5)$$

$T\Delta S$ is generally calculated using classical statistical thermodynamics and normal-mode analysis. Because of the entropy calculations for large systems being extremely time-consuming, we applied only 40 snapshots taken at an interval of 50 ps from the final 2000 ps of the MD simulation for the entropy contribution. Each snapshot was minimized with a distance dependent dielectric function $4R_{ij}$ (the distance between two atoms) until the root-mean-square of the energy gradient was lower than 10^{-4} kcal/mol/Å².

2.4. Residue-Inhibitor Interaction Decomposition. On account of the huge demand of computational resources for PB calculations, the interaction between TMC114 and each HIV-pr residue was computed using the MM-GBSA decomposition process applied in the mm_pbsa module in AMBER10. The

binding interaction of each inhibitor-residue pair includes four terms: van der Waals (ΔE_{vdw}) contribution and electrostatic (ΔE_{ele}) contribution in the gas phase, polar solvation (ΔG_{pol}) contribution, and nonpolar solvation (ΔG_{nopol}) contribution.

$$\Delta G_{\text{inhibitor-residue}}$$

$$= \Delta E_{\text{vdw}} + \Delta E_{\text{ele}} + \Delta G_{\text{pol}} + \Delta G_{\text{nopol}} \quad (6)$$

The polar contribution (ΔG_{pol}) to solvation energy was calculated by using the GB (Generalized Born) module and the parameters for the GB calculation were developed by Onufriev et al.⁴⁰ All energy components in eq 6 were calculated using 50 snapshots from the last 2.0 ns of the MD simulation. The hydrogen bonds (H-bonds) were analyzed using the ptraj module of the AMBER10 program. Formation of the H-bonds depends on the distance and angle cutoff as follows: (a) distance between proton donor and acceptor atoms were ≤ 3.5 Å, and (b) the angle between donor-H \cdots acceptor was $\geq 120^\circ$. Graphic visualization and presentation of protein structures were done using PYMOL.⁴¹

3. RESULTS AND DISCUSSIONS

3.1. Stability of Trajectories from rmsd. Exploring the effect of mutations on the conformational stability of the HIV-pr/TMC114 complexes, rmsd values for the HIV-pr C α atoms during the 20 ns production phase relative to the initial (minimized and equilibrated) structures were calculated and plotted in Figure 3. The rmsd plots indicate that the

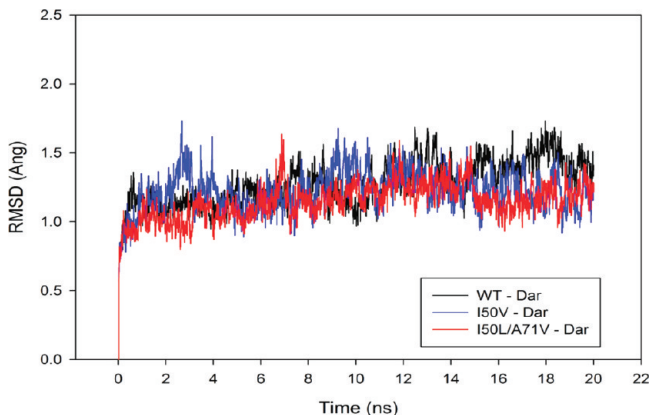


Figure 3. Root-mean-square displacement (rmsd) plot for backbone C α atoms relative to their initial minimized complex structures as a function of time.

conformations of the WT, single mutant (I50V), and double mutant (I50L/A71V) HIV-pr complexes are in good equilibrium. The trajectory of the I50V-HIV/TMC114 complex fluctuates more than the other two trajectories at around 3–5 ns; after that, it goes parallel to each other. According to the data obtained for the rmsd values of the three complexes, WT complex has a higher mean (1.27 Å) than the I50V mutant (1.22 Å) and I50L/A71V double mutant (1.14 Å), with a respective deviation of 0.16, 0.15, and 0.13 Å. The result signifies that rmsd of all three complexes were similar from the starting structures during the course of simulations with values around 1.0 to 1.7 Å ensuring stable trajectories. Figure S1 in the Supporting Information shows the rmsd plots for all (WT, I50V, and I50V/A71V) apo type HIV-pr and indicates that the conformations for all apo type have also achieved equilibrium.

There is no distinct changes/fluctuations in the apo form for all type HIV-pr and were similar from the starting structures during the course of simulations with values around 1.0 to 1.8 Å ensuring stable trajectories.

3.2. Comparing the Apo Proteins from B-factor: WT vs Mutant.

In order to analyze the detailed residual atomic fluctuations, an isotropic temperature factor (B-factor) calculation has been performed for the apo HIV-pr structure as illustrated in Figure 4a. For the given HIV-pr, the B-factor

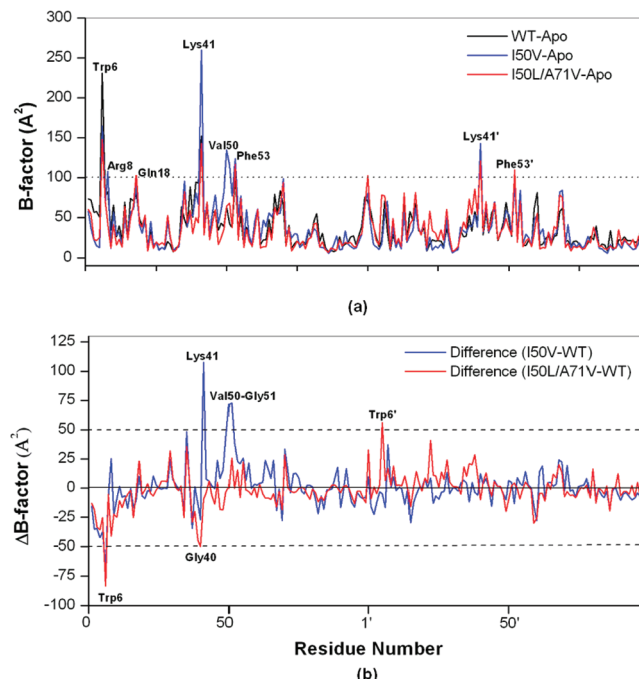


Figure 4. (a) B-factor of backbone atoms versus residue number of the WT, I50V, and I50L/A71V HIV-pr apo structures and (b) difference of B-factor values from molecular dynamics (MD) simulation for WT and mutant HIV-pr simulation of the apo protein (mutant B-factor – WT B-factor). The residues with an absolute difference larger than 50 Å 2 are labeled by two cutoff dashed lines.

difference between chain A and chain B may be due to the monoprotonation of ASP25' in chain B. The flexibility of the apoprotein in chain-A is greater in the case of I50V, particularly in the flap regions. Residue Arg8, contributing to the binding energetically favorably,⁴² is located in one of the most distinct regions of the protease molecule, i.e., dimer interface. In both chains for I50V-HIV-pr, Arg8 has a higher mobility as compared to WT and I50L/A71V. It is also confirmed from the B-factor values that the fulcrum residues are less affected due to the mutations in the protein backbone. Residues Gly16 and Gly17 in both chains for WT have significant higher mobility than the mutant duo I50V and I50L/A71V.

A difference of B-factors may provide direct insights into the structural fluctuation of different regions of WT and mutant HIV-pr. The difference in the isotropic temperature factor between the mutants and WT HIV-pr for each residue is shown in Figure 4b. The major changes in B-factor occur between WT and mutant HIV-pr for the residues in the dimer interface region (6, 8 and 6', 8'), flap elbow of the chain-A (35, 37, 39–41), and flap of the chain-A (49–52). The residues with an absolute difference larger than 50 Å 2 were taken as the most fluctuating residues and are labeled by two cutoff lines as shown

in the Figure 4b. It is noted that several other regions exist in which WT and mutant HIV-pr have different B-factors. In summary, by comparison of the B-factors between WT and mutant HIV-pr, a difference in the fluctuation of several amino acids was found, and this especially includes those residues at the flap tips, flap elbows, and dimer interface regions. Hence, the difference in the B-factors for the above-mentioned residues may affect the structural fluctuations of the protein and binding affinity for the substrate/inhibitor, consequently affecting the drug resistance behavior.

3.3. Local Fluctuations for Apo Proteins. Concerning the local structural differences between WT and mutant HIV-pr, the flap movement is particularly important to explore. It is well-known that flap dynamics affects both the inhibitor binding and enzyme catalysis of HIV-pr. Moreover, several mutations affect flap dynamics. For example, L90M and V82F/I84V mutations open the flap a bit more in the mutant than the WT,^{43,44} whereas M46I mutation makes the flap more closed.⁴⁵ In order to probe the extent of flap dynamics, usually the distance between the flap tip (Ile50 and Ile50') and the catalytic Asp residues (Asp25 and Asp25') was calculated. Estimation of the Ile50-Asp25 or the Ile50'-Asp25' distance was believed to be more realistic than the measure by monitoring the flap tip–tip (Ile50-Ile50') distance because the flap tip–tip distance can be affected by both flap tip curling and flap asymmetry. We have used several of these parameters to enquire the extent of flap motion in the current study.

3.3.1. Distance between Flap Tips ($\text{Ile}50\text{C}\alpha-\text{Ile}50'\text{C}\alpha$). The distance between the two $\text{C}\alpha$ atoms of Ile50 and Ile50' measures the distance between flap tips in both chains. The frequency distribution plot for flap tip–tip distance is shown in Figure 5.

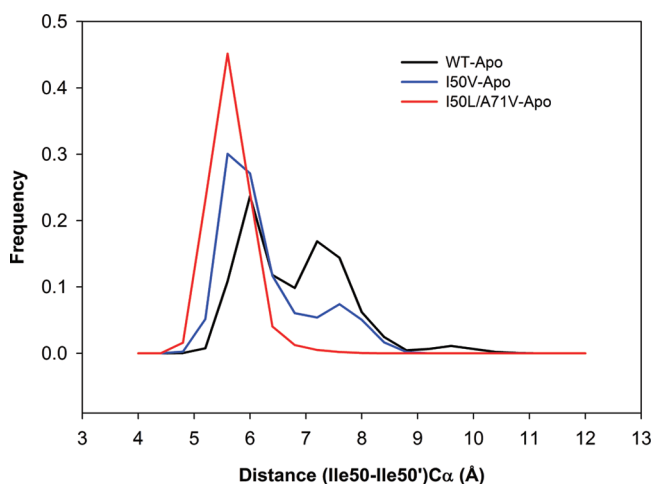


Figure 5. Histogram distributions of $\text{Ile}50-\text{Ile}50'$ distance for WT, I50V mutant, and I50L/A71V double mutant HIV-pr simulation of the apo protein.

It is clearly seen that with respect to $(\text{Ile}50-\text{Ile}50')$ $\text{C}\alpha$ distance, WT and I50V mutants assemble two different types of structures as compared with the I50L/A71V double mutant. For the double mutant, the distribution has one peak around 6 Å, whereas for WT and I50V mutants, the main peak locates around 6 Å, and the other minor around the 7–8 Å region. The mean and standard deviation (SD) of WT distribution are 7.0 Å and 0.92 Å, of I50V mutant are 6.45 Å and 0.8 Å, and those of the double mutant are 5.85 Å and 0.37 Å, respectively. While considerable overlaps exist in the three distributions, the

distance between the flap tips were recognized to fluctuate more in the case of WT and I50V than in the double mutant I50L/A71V. Hence, the mean of the double mutant structure is significantly less (1.15 Å) than the WT, suggesting that there is a close movement of flaps in I50L/A71V as compared to WT– and I50V–HIV-pr structures and probably making the active site volume smaller.

3.3.2. Flap Tip to Active Site ($\text{Ile}50-\text{Asp}25$) $\text{C}\alpha$ Distance. The distance between the flap tips ($\text{Ile}50\text{C}\alpha$ and $\text{Ile}50'\text{C}\alpha$) to the catalytic aspartates ($\text{Asp}25\text{C}\alpha$ and $\text{Asp}25'\text{C}\alpha$) of the active site was also measured from the simulation. The time series plot and the histogram distributions are shown in Figures 6a–d for chains A and B, respectively. These results reveal that the distances between the flap tip and catalytic site in chains A and B are clearly different for the double mutant I50L/A71V structures with smaller distance values compared to the WT and I50V mutant structures. According to Figure 6a, in chain-A for WT and I50V, there is considerable overlapping of the two distributions, whereas for I50L/A71V–HIV-pr, the distribution is quite different from those of WT and I50V. The mean and SD of WT (I50V) are 14.62 (14.20) Å and 0.98 (1.04) Å, respectively; whereas for the double mutant I50L/A71V, the mean and SD are only 13.51 Å and 0.83 Å, respectively. The mean of the distribution for I50L/A71V is smaller by 1.11 Å than WT and 0.69 Å than I50V. Moreover, chain-B (Figure 6b) also displays different conformational sampling for I50L/A71V as compared to WT and I50V. The mean and SD of WT (I50V) are 14.84 (14.02) Å and SD is 0.87 (0.70) Å respectively. Whereas, for the double mutant I50L/A71V, the mean and SD are 13.14 Å and 1.04 Å, respectively. Thus, the mean of the distribution for I50L/A71V in chain B differ by ~1.7 Å from WT and ~0.9 Å from I50V. The results indicate the smaller distance between the active site to flap residues in I50L/A71V than in WT and I50V. This result also complements with the tip–tip distance that suggests a close movement of flaps in I50L/A71V as compared to WT and I50V structures, probably making the active site smaller in volume. The reduced active site conformations of I50L/A71V due to the flap dynamics behavior may enhance the binding of an inhibitor to the active site region. This may be due to the increase in the van der Waals (vdw) contacts between the inhibitor and protein residues. For the clarification, we have also calculated the binding energy of the complexes, which will be discussed to correlate the present data.

3.3.3. Analysis of the TriCa Angle. In order to explain the flap dynamics behavior of the protein, Schiffer et al. introduced the term flap curling of the TriCa angles involving the residues in the flap tip or nearby region. It is known that the flap curling in and out behavior makes the protein opened and closed states, respectively, in order to access the substrate/inhibitor.⁴⁶ The simulation study by Rick et al. also explained the flap tip curling in prior to the opening event.⁴⁷ Curling in starts with the large change in the Φ and Ψ torsion values of residues 48–52 and fold back onto themselves to lead a bent L structure. We have used this term of flap curling to explain our observations of the MD studies using two angles ($\text{Gly}48-\text{Gly}49-\text{Ile}50$) and ($\text{Gly}49-\text{Ile}50-\text{Gly}51$) for the consideration as TriCa angle in the flap tip region. Figure 7 shows the time series plot for angle $\text{Gly}48-\text{Gly}49-\text{Ile}50$ $\text{C}\alpha$ atoms, where TriCa angle seems to be more stable for I50L/A71V–HIV-pr than those for the WT– and I50V–HIV-pr. For WT, the trajectory spends more time in the lower values at around 9 ns and the period of 14–20 ns. However, the I50V mutant spends more time in the lower

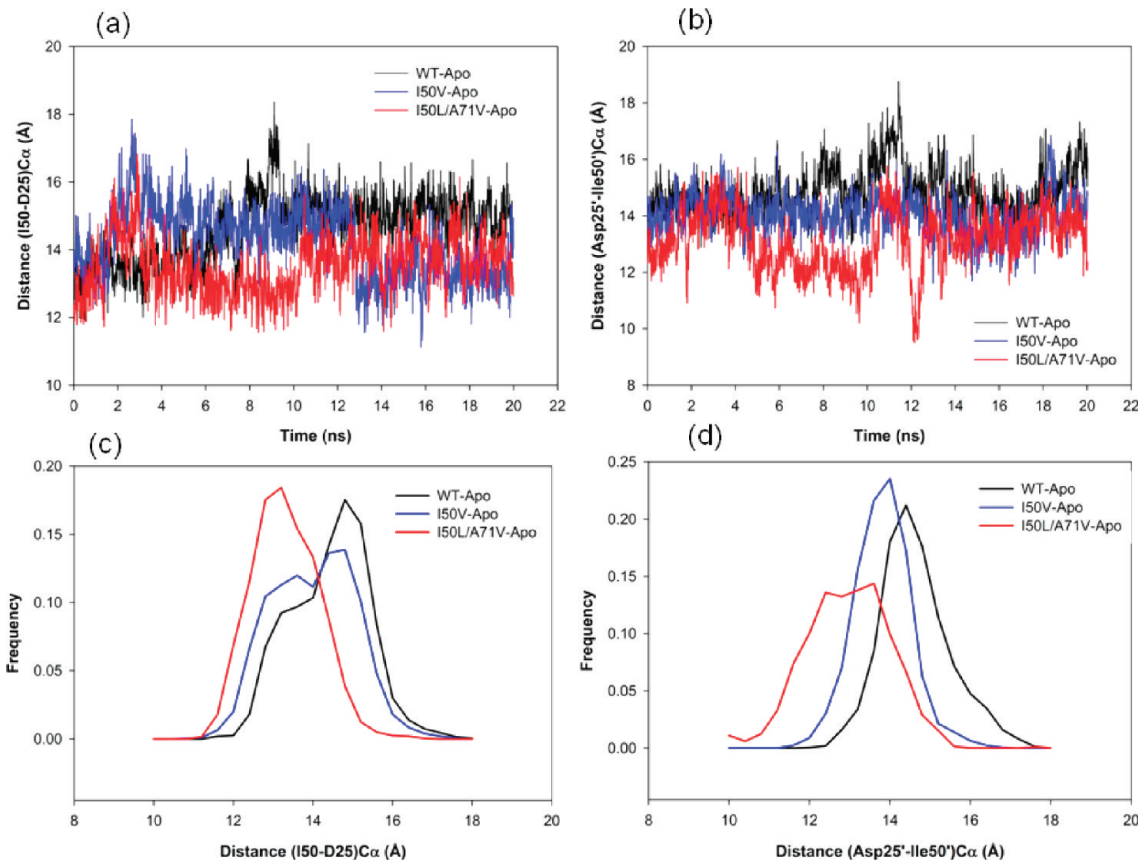


Figure 6. Variability of (a) the Ile50–Asp25 C_α distances; (b) the Ile50’–Asp25’ C_α distances of the apo WT, I50V mutant, and I50L/A71V double mutant HIV-pr. (c) Histogram distributions of Ile50–Asp25 distance; and (d) histogram distributions of Ile50’–Asp25’ distance for WT and all mutant HIV-pr simulation of the apo protein.

values in the initial but eventually overlaps with the WT in the end. Analyzing the frequency distribution plot for the TriCa angle 48–49–50, it was found that the distribution of the angle for WT and I50L/A71V overlaps substantially; however, the I50V distribution shows a difference as compared to the other two. The mean and SD of the TriCa angle Gly48–Gly49–Ile50 are 138.91° and 8.99° for WT distribution, 136.26° and 10.44° for I50V, and 142.59° and 6.13° for I50L/A71V. Hence, the SD of I50V is much higher than that of WT and especially than that of I50L/A71V, which is an indication of the higher mobility of the flap tips in the case of I50V.

By analyzing the frequency distribution plot (Figure 7d) for the other TriCa angle Gly49–Ile50–Gly51, it can also be found that the I50V mutant structures have different conformations as compared to WT and I50L/A71V. The distribution is almost overlapped for WT and I50L/A71V and is clearly different from that of the I50V mutant. The mean and SD of the TriCa angle for the WT (I50L/A71V) distribution are 97.65° (96.55) and 6.85° (4.81), respectively, whereas for the single mutant I50V, the mean and SD are 105.58° and 9.62°. Therefore, the mean of the two distributions of WT and I50L/A71V differ by ~8° and ~9° from that of the I50V mutant with wider value coverage for I50V. The time series plot (Figure 7b) also shows the higher fluctuations of I50V structures as compared to WT and I50L/A71V. Thus, finally it was noted that the I50V simulation samples different structures as compared to the WT and double mutant with respect to the flap tips mobility and curling, which is confirmed by the higher SD of both TriCa angles in the I50V–HIV-pr.

3.4. Comparing the Complexed Proteins from B-Factor: WT vs Mutant.

To get an insight to the detailed residual atomic fluctuations, an isotropic temperature B-factor calculation has also been performed for the complexed HIV-pr structure as illustrated in Figure 8a. Compared with Figure 4a, the flexibility of the apo protein is higher than that of the inhibitor bound protein, especially in the flap tip and flap elbow regions. This finding can simply be clarified in terms of binding between protease and inhibitor leading to the rigidity of the HIV-pr-TMC114 complex. This result also correlates well with the work reported by Zhu et al., where they observed the tight interaction between the fullerene-based inhibitor and the flaps leading to the closing of flexible flaps.⁴⁸

Overall, the three structure share similar B-factor distributions with a few exceptions. The average B-factor per-residue in the flap and active site binding region for the WT–, I50V–, and I50L/A71V–HIV-pr/TMC114 complexes are 31.03, 29.11, and 28.08 Å², respectively. The relatively smaller B-factor of the double mutant I50L/A71V complex may be explained by the relatively less conformational fluctuations and decreased flexibility. The decreased flexibility in the inhibitor-binding site leads to the decrease in K_m, i.e., an increase in the affinity of the enzyme for the inhibitor and stronger binding.⁴⁹ Thus, the lowest flexibility of I50L/A71V implies that the I50L/A71V–HIV-pr may have the highest binding affinity to TMC114 and tends to have the least drug resistance behavior.

All three complexes show similar trends of dynamic features. Regions around catalytic Asp25 and Asp25' show a rigid behavior, which is in line with the experimental⁵⁰ and

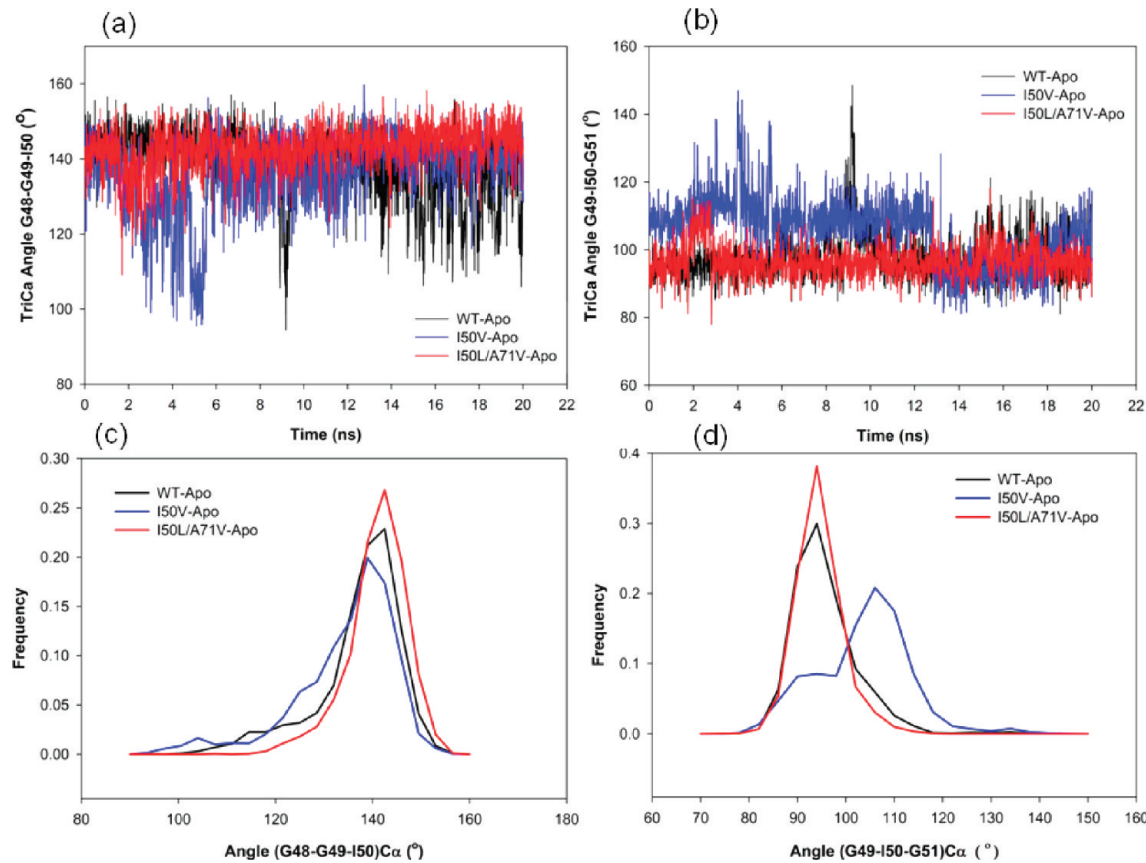


Figure 7. Variability of (a) the Gly48–Gly49–Ile50 TriCa angles and of (b) the Gly49–Ile50–Gly51 TriCa angles of the apo WT, I50V mutant, and I50L/A71V double mutant HIV-pr. (c) Histogram distributions of Gly48–Gly49–Ile50 TriCa angles; and (d) histogram distributions of Gly49–Ile50–Gly51 TriCa angles for WT and all mutant HIV-pr simulation of the apo protein.

theoretical^{10,51} investigations. It was observed that four regions around 18 (18'), 41 (41'), 53 (53'), and 70 (70') show the highest dynamic fluctuations. The flap elbow region containing the residue Lys41(41') shows the highest flexibility. This also agrees with the study of Ishima et al.,⁵² where the authors observed these regions of highest flexibility based on the differences in the experimental crystal structures in combination with the MD results. The difference of temperature factors (B-factor) of the protein in its complexed form is shown in Figure 8b. The residues with absolute difference larger than 50 Å² were taken as the significant fluctuating residues and are labeled by two cutoff lines as shown in the figure. It can be seen that compared with the apo protein in Figure 4, the difference between WT and mutant is reduced for most of the residues. However, there are still significant differences for the residues Trp6, Gly16–17 (fulcrum of chain A), 41–42 (flap elbow of chain A), Trp6', Arg8', and Pro39'-Lys41' (flap elbow of chain-B).

3.5. Local Fluctuations for Complexed Structure. We have then examined several key local fluctuations of the complexes of the inhibitor with WT and mutant HIV-pr. These include (1) Asp25(25')–Ile50(50') and (2) Ile50–Ile50' distances, (3) TriCa angle in the flap region, which indicate flap dynamics and flap–active site movements, and (4) Asp25(25')–inhibitor distance, which will be an indicator of the protein–ligand motion.

3.5.1. Flap Tip to Active Site Distances. The Asp25–(Asp25')–Ile50(Ile50') distances were calculated from the MD trajectories and the observed results were compared with those of apo proteins. It was found that for chain-A the distribution was much narrower compared with the apo proteins. Moreover,

the distributions for WT–, I50V–, and I50L/A71V–HIV-pr/TMC114 complexes have significant overlap (Figure 9a). The means for flap tip active site residue are 14.19, 14.09, and 14.30, and the SD values are 0.41, 0.37, and 0.41 for WT–, I50V–, and I50L/A71V–HIV-pr/TMC114, respectively. This indicates that in the inhibitor-bound state, the distance between the flap tips and the active site did not differ significantly on mutation for chain-A. For chain-B, there is a substantial difference between the distributions as compared with chain-A (Figure 9b). The mean and SD of I50V (I50L/A71V) are 14.49 (14.43) Å and 0.58 (0.47) Å, respectively; while for the WT, the mean and SD are only 14.94 Å and 0.53 Å, respectively. Therefore, the mean of the distribution for WT differ by approximately 0.5 Å from I50L/A71V and I50V. In general, for all proteases (WT, I50V, and I50L/A71V), the average flap tip active site distance in chain-B is longer than that in chain-A.

3.5.2. Flap Tip–Flap Tip Distances. To explore the relative motion of the flap tips, the Ile50–Ile50' distance was examined. The difference between the complexed WT–, I50V–, and I50L/A71V–HIV-pr was found to be less and narrower than that of the apo HIV-pr (Figure 10). Although the Ile50–Ile50' distances are similar to each other in the complexed HIV-prs, as shown above, the differences do exist in the Asp25–Ile50' distances, which shows the different behavior of the two chains of a homodimeric protein like HIV-pr. This result is quite similar to the earlier study on the JE-2147 bound I47V mutant.⁵³

3.5.3. Analysis of the TriCa (Gly49–Ile50–Gly51) C_α Angle. The flap dynamics of the inhibitor bound proteases can be further analyzed by the TriCa angles in the flap tip region for all three

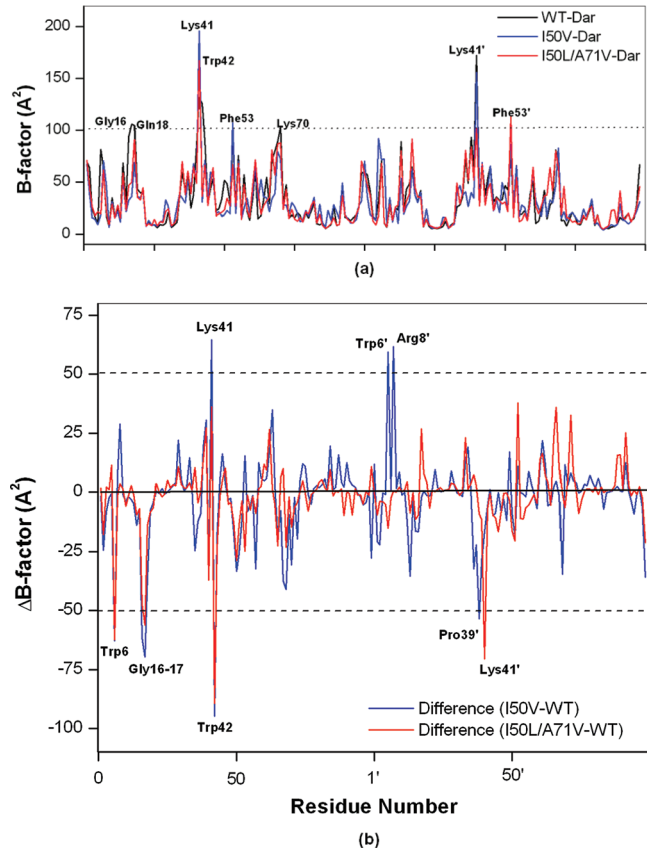


Figure 8. (a) B-factor of backbone atoms versus residue number of the WT, I50V, and I50L/A71V–HIV-pr–TMC114 complexed structures and (b) difference of B-factor values from molecular dynamics (MD) simulation for WT and mutant HIV-pr simulation of the complexed protein (mutant B-factor – WT B-factor). The residues with an absolute difference larger than 50 Å² are labeled by two cutoff dashed lines.

WT-, I50V-, and I50L/A71V–HIV-pr complexes. Looking at the distribution plot for the TriCa angle in Figure 11, we observed that the I50V and I50L/A71V mutant complexes have a single peak around ~110° and ~95°, respectively; while the WT has two peaks: the main peak at around 95° and the other at ~130°. The distribution is quite different as compared to the apo structures, where WT and I50L/A71V mutants are partially overlapped and is clearly different from the I50V mutant (Figure 7d).

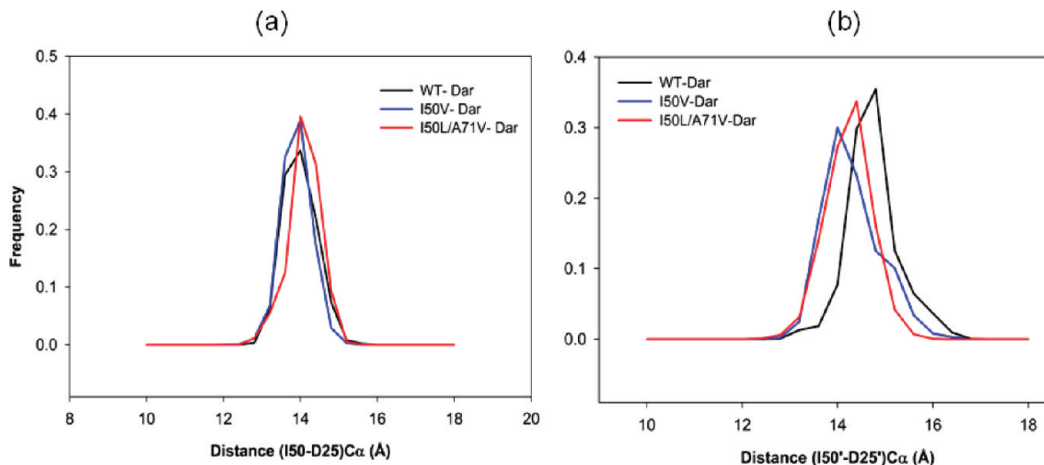


Figure 9. Histogram distributions of (a) Ile50–Asp25 distance and (b) Ile50'–Asp25' distance for WT, I50V mutant, and I50L/A71V double mutant HIV-pr simulation of the TMC114 complexed protein.

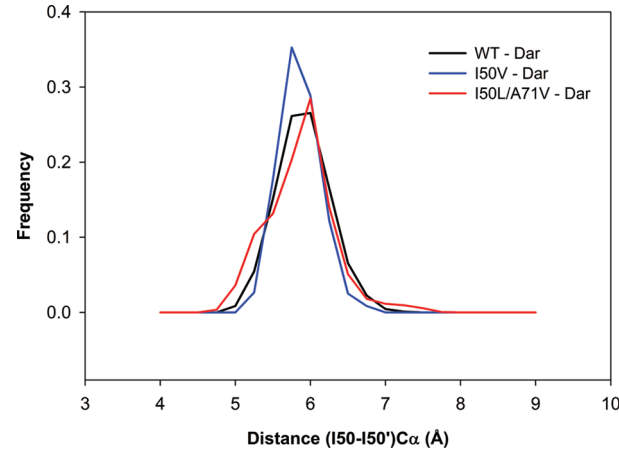


Figure 10. Histogram distributions of Ile50–Ile50' distance for WT, I50V mutant, and I50L/A71V double mutant HIV-pr simulation of the TMC114 complexed proteins.

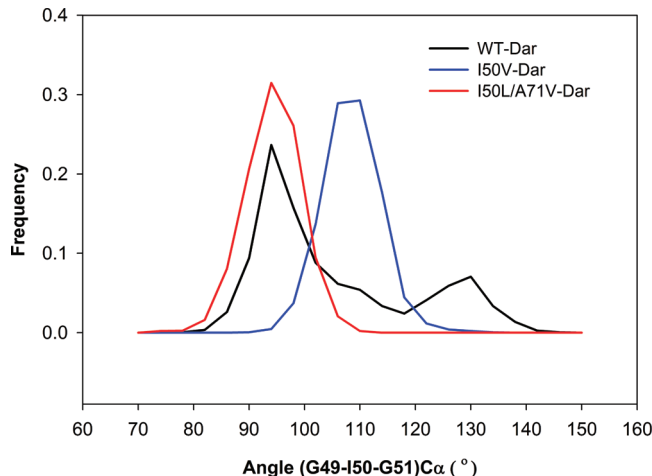


Figure 11. Histogram distributions of TriCa angle for WT, I50V mutant, and I50L/A71V double mutant HIV-pr simulation of the TMC114 complexed proteins.

The mean values of the TriCa angle for WT (I50V) distribution are 107.19° (110.54°), and SD is 14.33° (5.06°), whereas for the double mutant I50L/A71V, the mean and SD are 96.30°

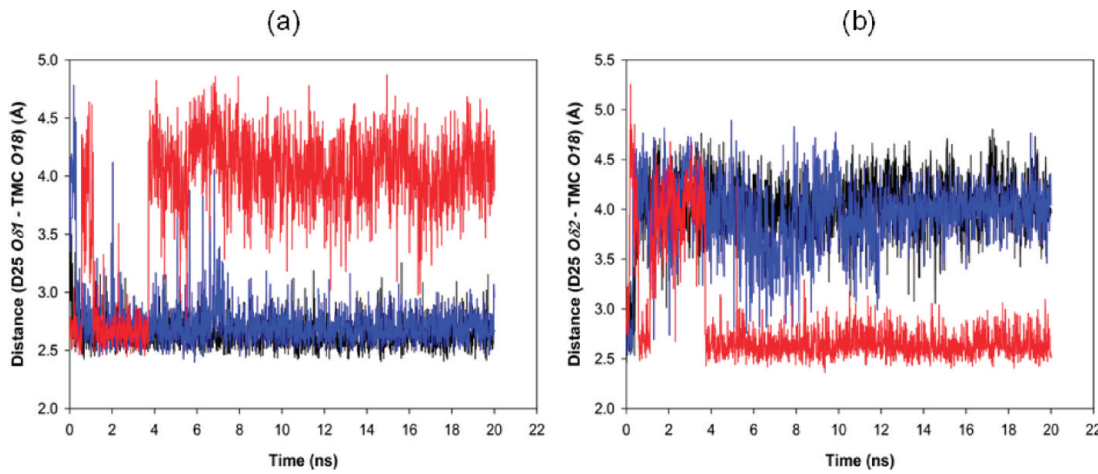


Figure 12. Time-series plot for the (a) protein–inhibitor (Asp25 OD1-TMC O18) interaction and (b) protein–inhibitor (Asp25 OD2-TMC O18) interaction for WT (black line), for I50V (blue line), and for I50L/A71V (red line).

and 4.90° . The mean values of WT and I50V are larger than that of the double mutant I50L/A71V complex by $\sim 11^\circ$ and $>14^\circ$, which implies the more curling out of the flap tips in WT and I50V than in the double mutant. However, the general pattern of the distribution frequency remains the same as apo protease even in the bounded complexes of the protein. The WT distribution also covers wider values than that of the other two distributions.

3.5.4. Protein (Asp25/Asp25')-Inhibitor (O18) Distance. Displacement of the inhibitor to the active site of the protein is coupled with the complex motion of the entire protein. In the crystal structure of the three proteases, WT, I50V, and I50L/A71V, residues in the flap tip, mostly Ile50/Val50/Leu50, do not have direct polar interactions with the TMC114 in 3 Å regions. However, the protein may bind to the inhibitor via a solvation bridge formed by a water molecule WAT-301. Additionally, the inhibitors are strongly bound to the protease with its OH_{isostere} (O18) to the catalytic Asp25/Asp25' OD1 and OD2 atoms. To get the protein–inhibitor distance, we have calculated the distances between the catalytic Asp duo (Asp25 and Asp25') and the O18 of TMC114. From the time series plot of distance between Asp25 OD1–TMC O18 (Figure 12), it was found to be almost always constant for WT (mean of 2.64 Å) and I50V (mean of 2.72 Å) as compared to their initial crystal structure distances of 2.58 Å and 2.59 Å, respectively. However, for the double mutant I50L/A71V, the distance was observed to be quite close between the two atoms from the beginning up to ~ 3.7 ns (except around 0.57 to 1.1 ns), but eventually around 4 ns, the distance goes high up to 4.8 Å. It was found from the crystal structure of double mutant I50L/A71V that the distance is 2.58 Å, while the obtained MD result has a mean of 3.84 Å. In contrast to the distance from OD1 to O18 of TMC114, Figure 12b shows that for double mutant I50L/A71V, the distance from OD2 to O18 eventually tends to be stable at 2.4 Å with a much shorter average (2.85 Å) than the other two cases (4.03 for WT and 3.94 for I50V). It suggests that there is always a flip-flop of the interaction between the catalytic Asp25 OD1/OD2 atoms and O18 of TMC114. This may be due to the effect of the mutation A71V from the double mutant, where the change from Ala71 to Val modifies the H-bonding pattern between the four antiparallel β -sheets connecting the Asp25 site to Val71. The change in the H-bonding pattern induces the rearrangement of β -sheets and finally affects the dynamics of Asp25 residues. The route

of propagation of the H-bonding and the change in dynamics can be observed from Figure 13. The mutation of Ala71 to

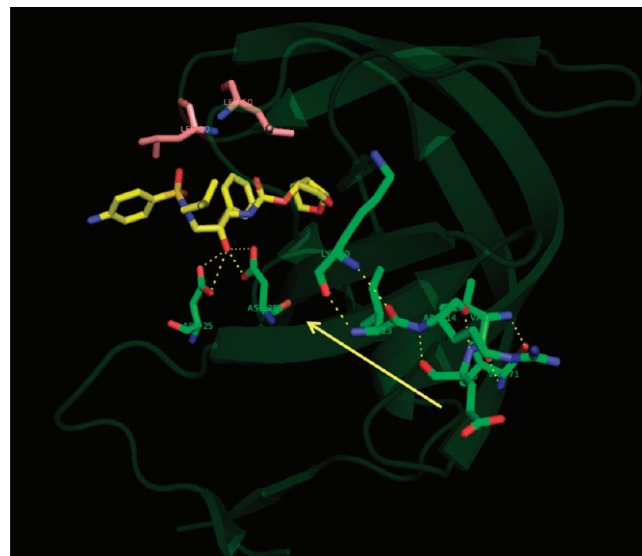


Figure 13. Schematic view of H-bond propagation in the double mutant I50L/A71V and Asp25(25')-TMC114 flip-flop interaction. Arrow shows the route of propagation.

valine requires more space to accommodate valine's bulkier side chain, which is oriented toward the enzyme interior. These requirements are met by a shift of the 70–71 main chain away from the loop encompassed by residues 92–93.¹⁶ The flip-flop interactions justify that the inhibitor is always bound to either of the OD1/OD2 atoms of Asp25, making the binding stronger in I50L/A71V as compared to WT and I50V.

3.6. Total Binding Free Energies. In order to gain insight to the contribution spectrum of binding energy for TMC114, with WT, I50V mutant, and I50L/A71V double mutant, absolute binding free energies are calculated for all the complexes using the MM-PBSA method. Contributions of the binding free energies of complexes WT, I50V, and I50L/A71V are summarized in the Table 1 and Figure 14. As shown in the figure and table, the binding free energies of WT, I50V, and I50L/A71V complexes are -15.33 , -10.88 , and -18.65 kcal/mol, respectively, which suggests that the I50L/A71V double mutant

Table 1. Binding Free Energy Components for the Protein–Inhibitor Complex by Using the MM-PBSA Method^a

component ^b	WT		I50V		I50L/A71V	
	mean	SD ^c	mean	SD ^c	mean	SD ^c
ΔE_{ele}	-42.34	5.61	-39.17	5.61	-47.86	6.96
ΔE_{vdw}	-63.87	3.36	-62.78	4.33	-64.29	3.43
ΔG_{np}	-6.98	0.13	-6.91	0.10	-7.00	0.11
ΔG_{pb}	71.19	3.47	70.12	4.40	73.18	5.24
ΔG_{pol}	28.85	4.41	30.95	3.67	25.32	4.65
ΔG_{total}	-42.00	3.69	-38.74	4.17	-45.98	4.21
$-T\Delta S$	26.67	4.88	27.86	6.63	27.33	7.80
ΔG	-15.33	6.11	-10.88	7.83	-18.65	8.86
ΔG_{exp}	-15.20 ^d		-11.90 ^e			
	-13.20 ^e					

^aAll values are given in kcal/mol. ^bComponent: ΔE_{ele} , electrostatic energy in the gas phase; ΔE_{vdw} , van der Waals energy; ΔG_{np} , nonpolar solvation energy; ΔG_{pb} , polar solvation energy; $\Delta G_{\text{pol}} = \Delta E_{\text{ele}} + \Delta G_{\text{pb}}$; $T\Delta S$, total entropy contribution; $\Delta G_{\text{total}} = \Delta E_{\text{ele}} + \Delta E_{\text{vdw}} + \Delta G_{\text{pb}}$; $\Delta G = \Delta G_{\text{total}} - T\Delta S$. ^cStandard error of mean values. ^dExperimental binding free energies are calculated using K_i , which are obtained from King et al.⁵⁵ ^eFrom ref 4.

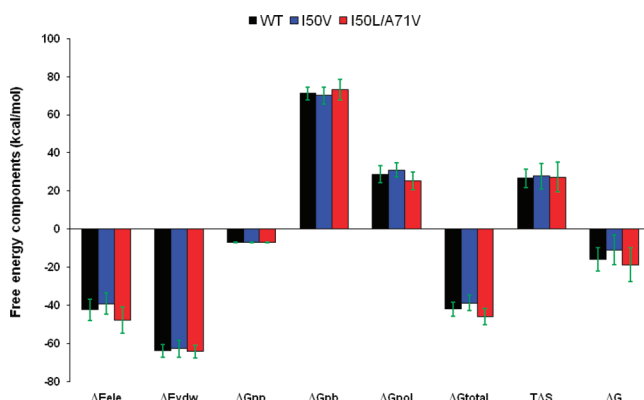


Figure 14. Energy components (kcal/mol) for the binding of TMC114 to the WT, I50V, and I50L/A71V. ΔE_{ele} , electrostatic energy in the gas phase; ΔE_{vdw} , van der Waals energy; ΔG_{np} , nonpolar solvation energy; ΔG_{pb} , polar solvation energy; $\Delta G_{\text{pol}} = \Delta E_{\text{ele}} + \Delta G_{\text{pb}}$; $T\Delta S$, total entropy contribution; $\Delta G_{\text{total}} = \Delta E_{\text{ele}} + \Delta E_{\text{vdw}} + \Delta G_{\text{int}} + \Delta G_{\text{pb}}$; $\Delta G = \Delta G_{\text{total}} - T\Delta S$. Error bars in green solid line indicates the difference.

HIV-pr has the strongest binding to the TMC114. The present results for the WT– and I50V–HIV-pr/TMC114 agree well with the available experimental affinities (-15.20 and -11.90 kcal/mol).^{5,54,55} In line with the previous studies,⁶ the binding affinity of the mutation I50V to TMC114 decreases by 4.45 kcal/mol compared to the WT complex, resulting in the drug resistance to the inhibitor; however, for the double mutation I50L/A71V complex, the binding affinity is increased by 3.32 kcal/mol. The results indicate that the mutant I50V induces weaker binding to TMC114, whereas the double mutant I50V/A71V enhances the binding affinity to TMC114. Although Yanchunas et al. showed that the mutant I50L/A71V exhibits increased binding to a number of protease inhibitors (except for atazanavir) relative to wild-type enzymes,¹⁴ there is no report on the effect of the double mutant on the HIV-pr's binding to TMC114. The enhanced binding affinity implies that the double mutant I50L/A71V may be well adapted by the TMC114.

The errors associated with calculated ΔG are reported now in Table 1. After taking into account the errors, the results in Table 1 still remain the same sequence as when excluding the

errors. As shown in Table 1, the experimental binding affinity difference between WT and I50V–HIV was 1.3–3.30 kcal/mol, which was determined to induce rather different performance to the TMC. The present results show that the binding affinity of the double mutant I50L/A71V is different from that of WT by -3.32 kcal/mol (-0.6 kcal/mol after taking error bars), and from that of the I50V by -7.8 kcal/mol (-6.7 kcal/mol after error bars), which will lead to different performance of the TMC114.

Comparisons of the free energy components between the WT complex and the single and double mutant complexes are carried out to explicate their interaction mechanism. In accordance with the energy components of the binding free energy in Table 1 and Figure 14, for all three HIV-pr-inhibitor complexes, van der Waals and electrostatic interactions in the gas phase provide the major favorable contributions to the inhibitor binding. Nonpolar solvation energies (ΔG_{np}), resulting from the burial of TMC114 solvent accessible surface area, also have favorable contributions to the binding affinity and are similar to each other in all of the three cases. Conversely, polar solvation energies (ΔG_{pb}) and entropy components ($-T\Delta S$) create the unfavorable contribution to the binding energy.

The relatively small nonpolar solvation energies among the three systems indicate that the packing of the cavity region is quite closed in all the systems. The I50V mutation shows a binding decrease due to electrostatic energy by about 3.17 kcal/mol and van der Waals energy by 1.09 kcal/mol relative to the WT, complementing the resistance of I50V to TMC114. This is in accordance to the previously published data of 4.42 and 0.92 kcal/mol for electrostatic and van der Waal's energy, respectively.⁶ For the case of double mutant I50L/A71V, all the energy components are more favorable for its binding to TMC114 except for the polar solvation energy ΔG_{pb} and $T\Delta S$ of the system relative to the WT complex. The double mutant I50L/A71V results in binding enhancement in terms of electrostatic energy and van der Waals by about -5.52 and -0.42 kcal/mol in the gas phase and binding decrease in ΔG_{pb} by about 2.0 kcal/mol and $T\Delta S$ by about 1.06 kcal/mol relative to the WT.

3.7. Structure-Binding Affinity Relationship Analysis.

To understand the effect of the two mutations on the interaction between the HIV-pr with TMC114 and to analyze the source of drug resistance, the analysis of structure and binding mode has been accomplished. The binding free energy was decomposed into inhibitor–residue pairs to create an inhibitor–residue interaction spectrum, shown in Figure 15. The approach of the residue decomposition method is enormously useful to explain the drug-resistant mechanism at atomistic detail and also helpful to locate the contribution of an individual residue to the protein–inhibitor interactions as well.¹⁸ It shows that the interaction spectra of three complexes are similar to each other. Overall, the major interaction comes from a few groups around Ala28/Ala28', Gly49/Gly49', Ile50/Ile50' (Val50/Val50'), and Ile84/Ile84'. These groups of interaction consist at least of 12 residues in total with the binding energy of more than 1 kcal/mol. Figure 16 shows the decomposition of ΔG values on a per-residue basis into contributions from van der Waals (ΔE_{vdw}), the sum of electrostatic interactions in the gas phase and polar solvation energy ($\Delta G_{\text{pol}} = \Delta E_{\text{ele}} + \Delta G_{\text{pb}}$), and nonpolar solvation energy (ΔG_{np}) for residues with $|\Delta G| \geq 1.0$ kcal/mol for all the three complexes. Table 2 further exemplifies the contributions of per-residue into those from backbone atoms and those from side chain atoms. Figure 17 describes the geometries of TMC114 in the binding complex with the relevant residues, which interact robustly with

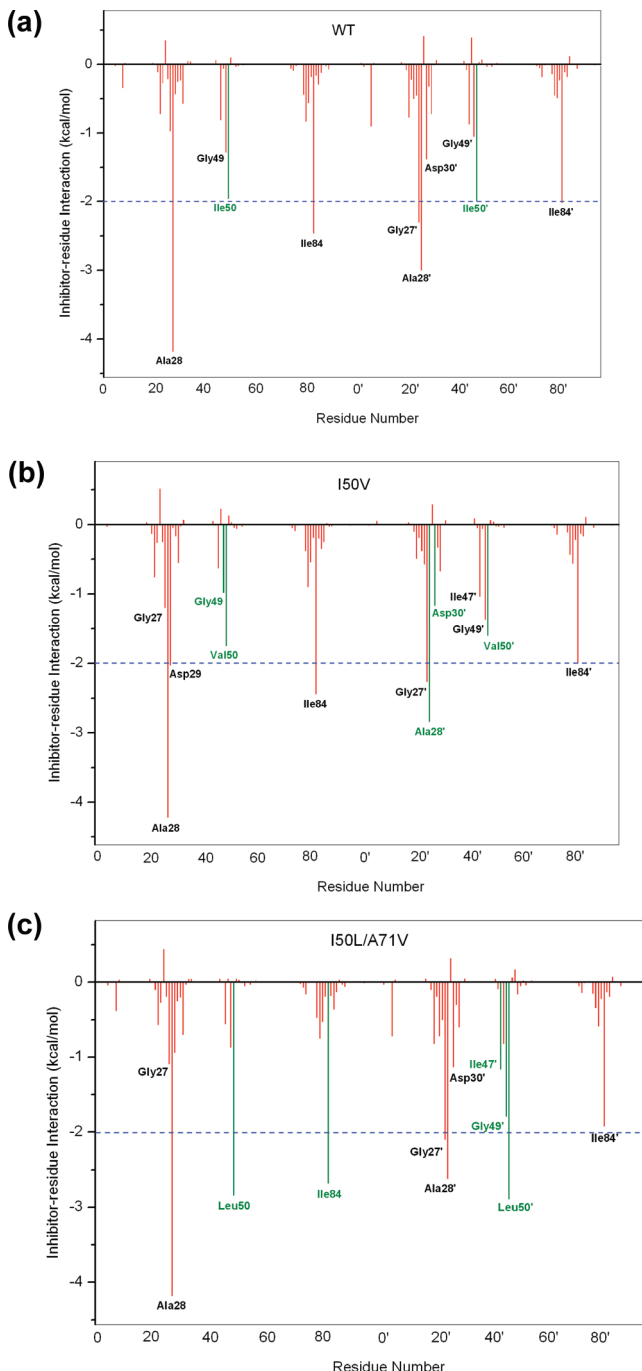


Figure 15. Decomposition of ΔG on a per-residue basis for the protein–inhibitor complex: (a) WT, (b) I50V, and (c) I50L/A71V.

TMC114 by using the lowest-energy structures from the MD simulation. Hydrogen bonds (H-bond) were analyzed on the basis of the trajectories with water molecules of the MD simulations (Table 3) to complement the energetic analysis.

For all twelve residues except for the Ile50'/Val50' shown in Figure 16a and Table 2, the main forces driving for the binding of TMC114 to HIV-pr are van der Waals energy (ΔE_{vdw}), the sum of electrostatic and polar solvation energies (ΔG_{pol}), and approximately -0.1 kcal/mol of nonpolar solvation energies (ΔG_{np}). For the Ile50'/Val50' residue, the favorable forces are van der Waals and nonpolar solvation energies, and ΔG_{pol} has an unfavorable contribution of 0.16 kcal/mol. Taking the WT–HIV-pr as an example, we again investigated the inter-

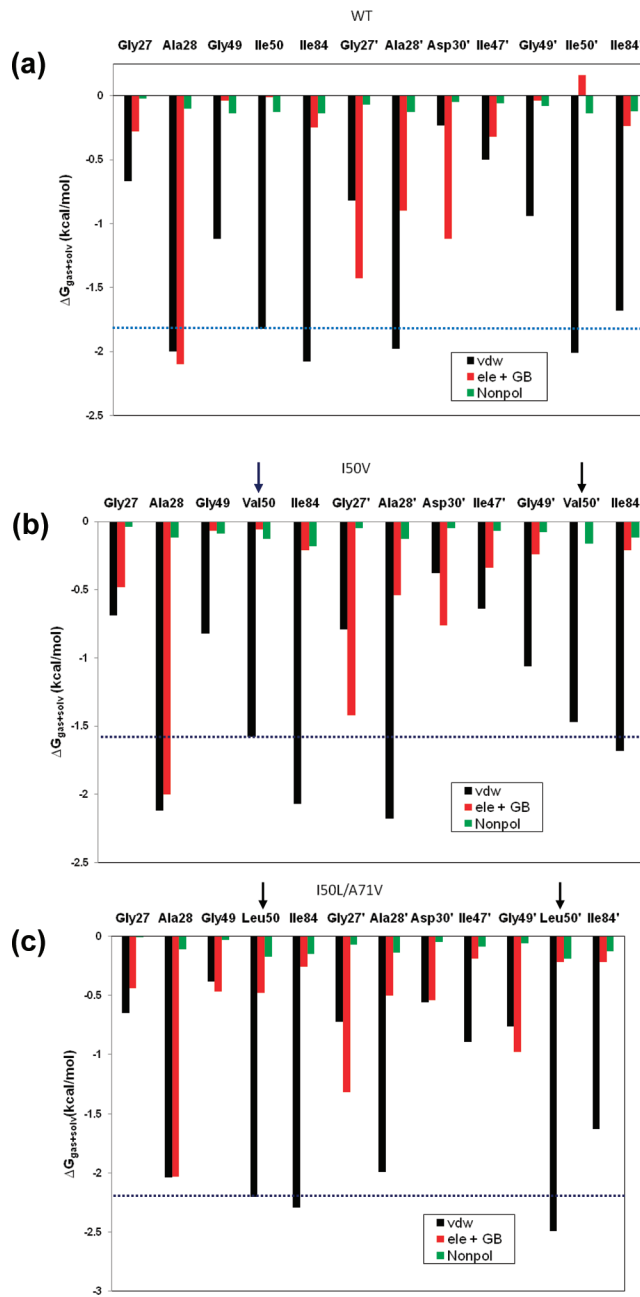


Figure 16. Decomposition of ΔG on a per-residue basis into contributions from the van der Waals energy (vdw), the sum of electrostatic interactions and polar solvation energy (ele + GB), and nonpolar solvation energy (np) for the residues of $|\Delta G| \geq 1.0$ kcal/mol: (a) WT, (b) I50V, and (c) I50L/A71V complexes.

actions between the main residues and the TMC114. For residue Ala28, the main force that directs the binding of TMC114 to the HIV-pr includes ΔE_{vdw} and ΔG_{pol} by -2.0 and -2.1 kcal/mol, respectively. The van der Waals energy is likely to be due to the C–H \cdots O weak hydrogen bonds between the alkyl of Ala28 and the bis-THF of TMC114, whereas ΔG_{pol} comes from the positively charged side chain atoms of Ala28 and the negatively charged oxygen atom of bis-THF moiety of the inhibitor TMC114. Similar to Ala28 in chain-A of HIV-pr, the binding of Ala28' in chain-B to the TMC-114 is also mainly from van der Waals energy (-1.98 kcal/mol) and ΔG_{pol} (-0.90 kcal/mol). The van der Waals term is due to the C–H \cdots π interaction between the aniline of TMC114 and the

Table 2. Decomposition of ΔG on a Per-Residue Basis (GB)^a

residue	S_{vdw}	B_{vdw}	T_{vdw}	S_{ele}	B_{ele}	T_{ele}	S_{GB}	B_{GB}	T_{GB}	T_{SUR}	T_{GBTOT}
WT-TMC114											
Gly27	0.00	-0.67	-0.67	0.00	1.03	1.03	0.00	-1.31	-1.31	-0.02	-1.00
Ala28	-0.61	-1.39	-2.00	0.22	-2.03	-1.81	-0.01	-0.28	-0.29	-0.10	-4.19
Gly49	0.00	-1.12	-1.12	0.00	-1.25	-1.25	0.00	1.21	1.21	-0.14	-1.29
Ile50	-1.36	-0.46	-1.82	-0.47	0.36	-0.11	0.23	-0.13	0.10	-0.13	-1.97
Ile84	-1.92	-0.16	-2.08	0.16	-0.02	0.14	-0.29	-0.10	-0.39	-0.14	-2.47
Gly27'	0.00	-0.82	-0.82	0.00	-0.56	-0.56	0.00	-0.87	-0.87	-0.07	-2.31
Ala28'	-0.61	-1.37	-1.98	0.14	-0.70	-0.56	0.05	-0.39	-0.34	-0.13	-3.01
Asp30'	-0.25	0.02	-0.23	-2.76	-3.68	-6.44	2.91	2.41	5.32	-0.05	-1.39
Ile47 ^b	-0.41	-0.09	-0.50	-0.13	-0.19	-0.32	-0.03	0.03	0.00	-0.06	-0.88
Gly49'	0.00	-0.94	-0.94	0.00	-0.75	-0.75	0.00	0.71	0.71	-0.08	-1.06
Ile50'	-1.52	-0.49	-2.01	-0.32	0.20	-0.12	0.17	0.11	0.28	-0.14	-2.00
Ile84'	-1.55	-0.13	-1.68	0.06	-0.30	-0.24	-0.22	0.22	0.00	-0.12	-2.03
ISOV-TMC114											
Gly27	0.00	-0.69	-0.69	0.00	0.88	0.88	0.00	-1.36	-1.36	-0.04	-1.21
Ala28	-0.67	-1.45	-2.12	0.18	-1.92	-1.74	0.00	-0.26	-0.26	-0.12	-4.23
Gly49	0.00	-0.82	-0.82	0.00	-0.81	-0.81	0.00	0.74	0.74	-0.09	-1.00
Val50	-0.99	-0.59	-1.58	-0.46	0.54	0.08	0.16	-0.30	-0.14	-0.13	-1.76
Ile84	-1.90	-0.17	-2.07	0.11	-0.02	0.09	-0.21	-0.09	-0.30	-0.18	-2.45
Gly27'	0.00	-0.79	-0.79	0.00	-0.85	-0.85	0.00	-0.57	-0.57	-0.05	-2.27
Ala28'	-0.76	-1.42	-2.18	0.10	-0.31	-0.21	0.05	-0.38	-0.33	-0.13	-2.85
Asp30'	-0.27	-0.11	-0.38	-3.18	-3.19	-6.37	3.30	2.31	5.61	-0.05	-1.18
Ile47'	-0.52	-0.12	-0.64	-0.02	-0.09	-0.11	-0.08	-0.15	-0.23	-0.07	-1.05
Gly49'	0.00	-1.06	-1.06	0.00	-1.08	-1.08	0.00	0.84	0.84	-0.08	-1.38
Val50'	-0.94	-0.53	-1.47	-0.49	-0.01	-0.50	0.25	0.26	0.51	-0.16	-1.61
Ile84'	-1.56	-0.12	-1.68	0.00	-0.28	-0.28	-0.19	0.26	0.07	-0.12	-2.01
ISOL/A71V-TMC114											
Gly27	0.00	-0.65	-0.65	0.00	0.77	0.77	0.00	-1.21	-1.21	-0.01	-1.10
Ala28	-0.60	-1.44	-2.04	0.18	-1.96	-1.78	-0.04	-0.21	-0.25	-0.11	-4.19
Gly49 ^b	0.00	-0.38	-0.38	0.00	-1.10	-1.10	0.00	0.63	0.63	-0.03	-0.88
Leu50	-1.76	-0.44	-2.20	-0.64	-0.52	-1.16	0.32	0.36	0.68	-0.17	-2.85
Ile84	-2.13	-0.16	-2.29	0.17	-0.05	0.12	-0.30	-0.08	-0.38	-0.15	-2.69
Gly27'	0.00	-0.72	-0.72	0.00	-0.63	-0.63	0.00	-0.69	-0.69	-0.07	-2.11
Ala28'	-0.67	-1.32	-1.99	0.11	-0.23	-0.12	0.06	-0.44	-0.38	-0.14	-2.63
Asp30'	-0.23	-0.33	-0.56	-2.90	-3.23	-6.13	3.08	2.51	5.59	-0.05	-1.14
Ile47'	-0.73	-0.16	-0.89	0.01	0.15	0.16	-0.10	-0.25	-0.35	-0.09	-1.17
Gly49'	0.00	-0.76	-0.76	0.00	-1.98	-1.98	0.0	1.00	1.00	-0.06	-1.80
Leu50'	-1.59	-0.90	-2.49	-0.37	0.01	-0.36	0.29	-0.15	0.14	-0.19	-2.90
Ile84'	-1.50	-0.13	-1.63	0.10	-0.30	-0.20	-0.23	0.21	-0.02	-0.13	-1.93

^aEnergies shown as contributions from van der Waals energy (vdw), electrostatic energy (ele), polar solvation energy (GB), the nonpolar solvation energy (SUR) of side chain atoms (S), backbone atoms (B), and the total (T) of protein–inhibitor complex. Only residues of $|\Delta G| \geq 1.0$ kcal/mol were listed. All values are given in kcal/mol. ^bValues did not meet $|\Delta G| \geq 1.0$ kcal/mol.

alkyl of Ala28'. The N20 atom of TMC114 forms a H-bond with the carbonyl oxygen of Gly27 in the initial crystal structure via N–H···O. The H-bond is broken probably due to electrostatic repulsion ($T_{\text{ele}} = 1.03$ kcal/mol). The hydrophobic interaction with the van der Waals energy between Gly27 and TMC114 directs the binding. As shown in Figure 17, the H-bond analysis indicates that atoms O26 and O28 of the bis-THF group form three H-bonds with the main chain amides of Asp29 and Asp30, respectively. The H-bonds with a high percentage of occupancy indicate that the interactions between the two residues and TMC114 are relatively strong. Moreover, the residue-inhibitor interaction energies justify the presence of H-bonds between the bis-THF group and the side chain of the Asp29 and Asp30 residues (Table 3 and Figure 17). Similarly, the N1 atom of TMC114 forms a H-bond with the carbonyl oxygen of Asp30' through N–H···O. This analysis is in accordance to the strong side chain electrostatic energy ($S_{\text{ele}} =$

-2.76 kcal/mol) and backbone electrostatic energy ($B_{\text{ele}} = -3.68$ kcal/mol) in Table 2. However, the residue decomposition for Asp30' shows that the polar solvation energies considerably decrease the binding of WT-TMC114 by 5.32 kcal/mol. Thus, the total contribution from polar solvation energies and electrostatic energy is the key driving force for the binding of TMC114 to Asp30' (Figure 16a). Furthermore, the central phenyl in TMC114 interacts with the alkyl of the residues Gly49/Gly49' and Ile50/Ile50' through C–H···π. The bis-THF group of TMC114 interacts with the alkyl of the residue Ile84 via C–H···O, and aniline of TMC114 interacts with the alkyl of residue Ile84' through C–H···π. Thus, the van der Waals energy favors the binding of these six residues (Figure 16a). For Ile50/50' and Val50/50', although the main driving force to the binding is van der Waals energy with a small unfavorable ΔG_{pol} in cases of WT-TMC and ISOV-TMC (Figures 16a and 16b), a favorable ΔG_{pol} along with the van der

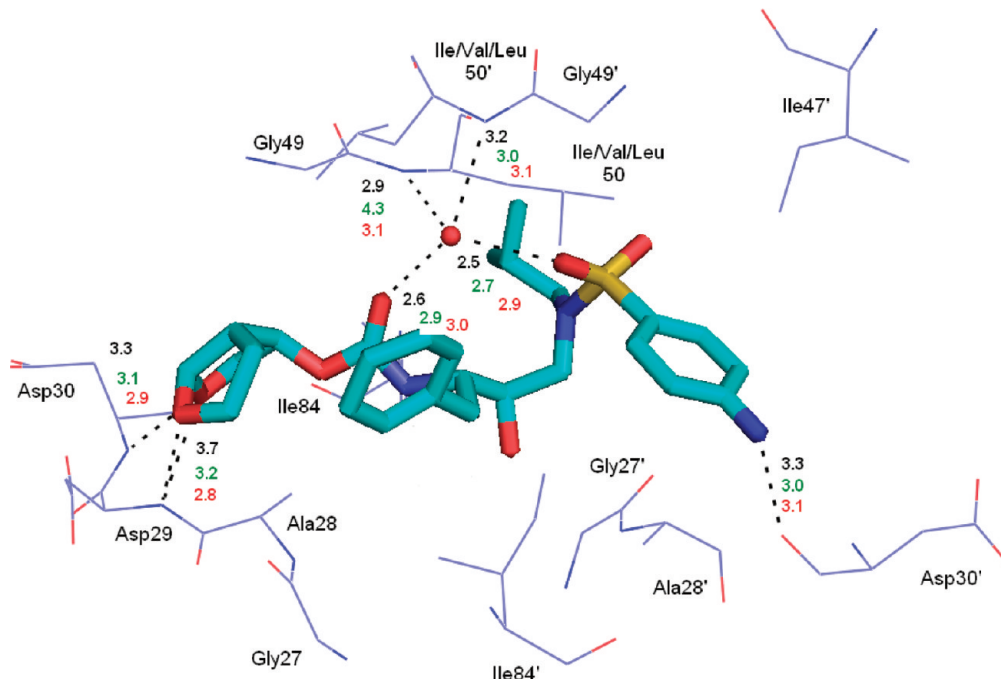


Figure 17. Geometries of residues with major interactions to TMC114 are plotted. Hydrogen bonds are shown in dashed black line with distances (black, WT; green, I50V; red, I50L/A71V). TMC114 is indicated in a stick representation, the oxygen of WAT-301 is indicated by a red sphere model, and the residues are shown in a line representation.

Table 3. Hydrogen Bonds Formed by TMC114 with the HIV-pr and with WAT-301^a

acceptor	donor	wild-type (WT)		I50V		I50L/A71V	
		distance (Å)	% occupancy	distance (Å)	% occupancy	distance (Å)	% occupancy
TMC114–O9	WAT-301–O–H			2.762 (0.14)	96.39		
TMC114–O10	WAT-301–O–H	2.831 (0.17)	99.17	2.864 (0.18)	98.37	2.796 (0.15)	99.60
TMC114–O22	WAT-301–O–H	2.834 (0.16)	98.59			2.806 (0.15)	99.85
WAT-301–O	Ile(Val/Leu)50’–N–H	3.080 (0.17)	92.72	3.068 (0.17)	94.86	3.070 (0.17)	91.58
WAT-301–O	Ile(Val/Leu)50’–N–H	3.109 (0.17)	88.00	3.191 (0.17)	69.50	3.076 (0.17)	92.52
TMC114–N1	Asp30’–N–H	3.125 (0.15)	90.85	3.125 (0.15)	88.98	3.097 (0.15)	95.59
TMC114–O26	Asp30–N–H	3.238 (0.16)	66.81	3.175 (0.16)	75.12	3.219 (0.16)	45.95
TMC114–O28	Asp29–N–H	3.103 (0.18)	80.35	3.115 (0.19)	73.69	3.108 (0.18)	51.79
TMC114–O26	Asp29–N–H	3.045 (0.17)	63.79	3.035 (0.17)	54.38	3.061 (0.17)	37.10
TMC114–N1	Asp29’–N–H	3.230 (0.15)	34.64	3.246 (0.15)	23.02	3.252 (0.14)	23.02

^aThe H-bonds are determined by the donor···acceptor atom distance of ≤ 3.5 Å and acceptor···H-donor angle of $\geq 120^\circ$.

Waals energy plays important roles in binding of TMC114 to I50L/A71V double mutant (Figure 16c).

3.8. Direct and Indirect Effects of Mutations on the Binding Affinity. According to T_{GBTOT} in Table 2 and Figure 15, the I50V mutant directly reduces the binding affinity by approximately 0.21 (Ile50 to Val50) and 0.39 (Ile50’ to Val50’) kcal/mol, which only accounts for 18% of the total loss of the binding affinity. In line with the larger opening of apo I50V–HIV-pr, the entropy effect decreases the binding affinity more than WT by 1.19 kcal/mol. In the I50V mutant HIV-pr, the replacement of isoleucine with valine results in a loss of a methyl group, which apparently decreases the interaction with the central phenyl of TMC 114 through C–H··· π , the size of the hydrophobic side chain and possible increase of the size of the active site with a reduced binding affinity to TMC114. According to Table 2, this change results in a decrease of van der Waals energy between Val50 and TMC114 by about 0.24 kcal/mol relative to the WT, which agree well with the result from Chen et al. with 0.39 kcal/mol.⁶ However, for

Val50’, the change shows a more significant decrease in van der Waals energy by 0.54 kcal/mol, which may be due to the lessening of C–H···O interactions between the Val50’ side chains and the O22 of TMC114. Figure 18d confirms that the C···O22 for I50V–HIV-pr is longer than those for WT and I50L/A71V–HIV-pr (4.1 vs 3.6 Å). The electrostatic energy in the present result is not as high as that of Chen et al. for Val50’ (T_{ele} , -2.03^6 vs -0.50 kcal/mol).

Table 2 and Figure 15 show that, besides the direct effects from the residues Val50 and Val50’, the residues Gly49, Ala28’, and Asp30’ also considerably decrease the binding affinity of I50V–HIV-pr to the inhibitor by 0.29, 0.16, and 0.21 kcal/mol, respectively, accounting approximately another 20% of the total binding loss. For the residue Gly49, the decreases of van der Waals ($\Delta T_{vdw} = 0.30$ kcal/mol) and electrostatic ($\Delta T_{ele} = 0.44$ kcal/mol) energies of the backbone are mainly responsible for its binding loss. For the residue Ala28’, the electrostatic interaction of the backbone is decreased by 0.39 kcal/mol. There exists one H-bond between the TMC114 and Asp30’

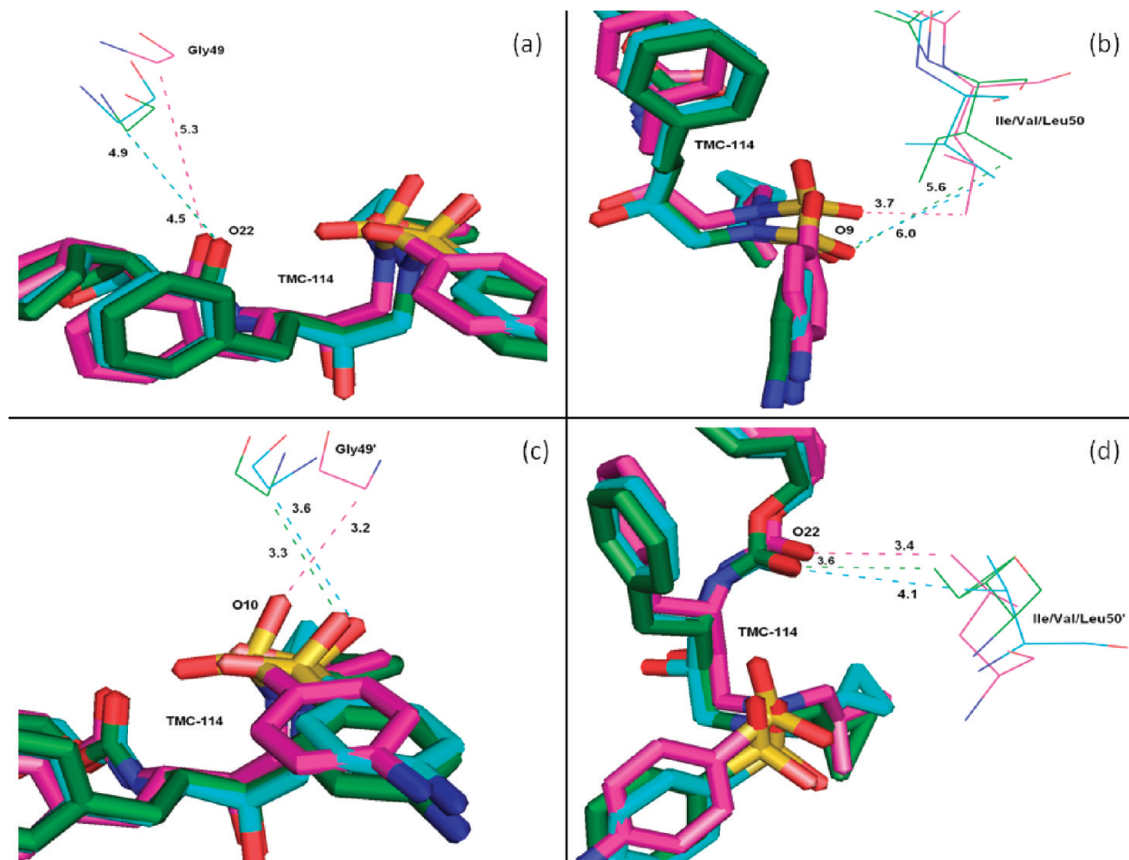


Figure 18. C–H...O interactions between the TMC114 and the flap residues (Gly49, Gly49', Ile/Val/Leu50, and Ile/Val/Leu50'). TMC114 in sticks is colored by the atom type, and residues are shown as lines (green, WT; blue, I50V; purple, I50L/A71V).

side chain carbonyl oxygen. This is in accordance to the favorable electrostatic interaction of TMC114 and the Asp30' side chain but is accompanied by the increase in polar solvation energy of Asp30' by about 0.36 kcal/mol relative to the WT, counterbalancing the favorable electrostatic energy. Hence, on the basis of the above structural energetic analysis discussed, we can conclude that the direct effects from Val50 and Val50', e.g., the decrease in van der Waals for both residues and the increase in polar solvation energy for Val50', with a few other residues, Gly49, Ala28', and Asp30', accomplish the drug resistance in the I50V mutant.

Table 2 further shows that the I50L/A71V mutant directly increases the binding affinity by approximately −0.88 (Ile50 to Leu50) and −0.90 (Ile50' to Leu50') kcal/mol, which accounts for 45% of the total gain of the binding affinity. The secondary mutation A71V does not have much direct effect on the binding. For the mutation from Ile50 to Leu50, the binding enhancement can be mainly attributed to the electrostatic by −1.05 kcal/mol and van der Waals by −0.38 kcal/mol, yet considerably being compromised by the increase of the polarization energy of 0.58 kcal/mol; whereas from Ile50' to Leu50', the contribution from the electrostatic is only −0.24 kcal/mol and the van der Waals term is significant by −0.48 kcal/mol. Besides the direct effects from the residues Leu50 and Leu50', the residue Gly49' considerably increases the binding affinity of I50L/A71V–HIV-pr to the inhibitor by −0.74 kcal/mol to which the electrostatic energy of Leu50's backbone contributes by −1.23 kcal/mol. According to Figure 18b–d, these enhancements are also consistent with the shortest distances of C–O10, C–O9, and C–O22 for Gly49', Leu50, and Leu50' of I50L/A71V–HIV-pr,

respectively, as compared to those of WT and I50V–HIV. Another two residues, Ile84 and Ile47', also increase the binding affinity by −0.22 and −0.29 kcal/mol, respectively, which can be mainly attributed to van der Waals terms (ΔT_{vdw} , −0.21 and −0.39 kcal/mol).

In the I50L/A71V double mutant HIV-pr, the isoleucine-to-leucine substitution places the methyl group in a different position without significant change in the conformation of the side chain. However, the alanine-to-valine substitution imposes the addition of two methyl groups to the backbone carbon in place of a single methyl, which changes the side chain conformation to be a bit bulkier and need more space to accommodate it toward the enzyme interior. Compared to the WT and I50V mutant, the I50L/A71V HIV-pr has less stability of the H-bonding between the Asp29/Asp30 with the O26 and O28 of bis-THF group. The occupancy of the H-bonding is reduced to less than 50% (Table 3). The change in H-bonding for I50L/A71V HIV-pr results in a reduction of polarity energies ($E_{ele} + T_{GB}$) of residue Asp30' by about 0.58 kcal/mol compared to the WT case (Figure 15c). Thus, the loss of H-bonding between TMC114 and the side chain of Asp30' (Asp29) and the polar solvation energies for Asp30' indirectly relate to the binding of I50L/A71V HIV-pr to TMC114. This may be an indirect effect of the mutations pair that can be related to the allosteric nature.

Hydrogen bonds formed between β -strands (connecting residues 71…64, 65…14, and 13…20) in both chains of the HIV-pr have been summarized in Table 4. It is noted that the change from Ala71 to Val71 in the cantilever region of the HIV-pr has not affected much the H-bond pattern, which can be

Table 4. Hydrogen Bonds Formed between β -Strands (Connecting Residues 71 \cdots 64, 65 \cdots 14, and 13 \cdots 20) in Both Chains of HIV-pr^a

acceptor	donor	wild-type (WT)		I50V		I50L/A71V	
		distance (Å)	% occupancy	distance (Å)	% occupancy	distance (Å)	% occupancy
Glu65-O	Arg14'-N-H	3.077 (0.18)	90.76	2.980 (0.16)	96.96	3.043 (0.19)	94.29
Glu65'-O	Arg14'-N-H	3.014 (0.19)	99.00	2.973 (0.15)	99.01	3.003 (0.18)	75.84
Arg14-O	Glu65-N-H	2.991 (0.17)	97.51	3.142 (0.17)	91.86	3.030 (0.18)	96.08
Arg14'-O	Glu65'-N-H	2.830 (0.16)	94.84	3.136 (0.17)	91.74	3.065 (0.19)	73.36
Val64-O	Ala/Val71-N-H	2.985 (0.16)	99.01	2.949 (0.14)	99.39	2.966 (0.14)	99.46
Val64'-O	Ala/Val71'-N-H	2.946 (0.14)	99.02	2.960 (0.14)	99.05	2.972 (0.14)	99.47
Ala71-O	Val64-N-H	2.932 (0.13)	99.84	2.981 (0.15)	99.33	2.935 (0.13)	99.86
Ala71'-O	Val64'-N-H	2.919 (0.13)	99.85	3.049 (0.15)	98.41	2.961 (0.14)	98.65
Lys20-O	Ile13-N-H	2.860 (0.11)	99.76	2.864 (0.11)	99.91	2.868 (0.11)	99.80
Lys20'-O	Ile13'-N-H	2.866 (0.11)	99.81	2.866 (0.11)	99.94	2.892 (0.11)	99.97
Ile13-O	Lys20-N-H	2.966 (0.14)	99.26	2.980 (0.14)	99.56	2.962 (0.15)	99.59
Ile13'-O	Lys20'-N-H	2.990 (0.15)	99.41	2.981 (0.15)	99.41	2.975 (0.14)	99.64

^aThe H-bonds are determined by the donor \cdots acceptor atom distance of ≤ 3.5 Å and acceptor \cdots H-donor angle of $\geq 120^\circ$.

seen with $\geq 90\%$ occupancy. However, the H-bond between the residues Arg14' and Glu65' has been reduced to an occupancy with $\sim 75\%$, which can still be stable enough for a H-bond to exist. This result confirms that mutation A71V does not have direct influence on the active site conformation and binding affinity. Rather, it has an allosteric effect on the binding affinity with change in the mobility of active site residues by H-bond propagation from the site of mutation to the active site region. The resultant change in conformation of the protein, may affect the binding affinity of the inhibitor TMC114 to the protease.

It was noted that during the 20 ns MD simulations, the water (WAT-301) that makes bridges between the inhibitor and flap tip residues Ile50/Ile50' was observed to be well maintained for all three protease systems. The water molecule WAT-301 in the investigated three HIV-pr-inhibitor complexes connects the inhibitor and protein via four H-bonds (Table 3 and Figure 17). According to Table 3, the occupancy of these four H-bonds is higher than 88%, except for the bond between the Val50' and WAT-301 in the case of the I50V mutant, where the occupancy is $\sim 70\%$. Regardless of the change in residues from isoleucine to valine in I50V or isoleucine to leucine in I50L/A71V, the mutations do not have a great impact on the stability of the function of WAT-301. This observation suggests that WAT-301 is hardly involved in the resistance of both I50V single and I50L/A71V double mutants to TMC114.

4. REMARKS ON FLAP DYNAMICS AND BINDING AFFINITY

The MD simulation results show that for the apo protein, there is a difference in dynamic motion of WT and mutant involving the residues in the dimer interface (Trp6 and Arg8), flap elbow (Gly40-Lys41), and flap tip (Ile/Val/Leu50-Gly51) regions. In the case of the complexed HIV-pr, the difference in dynamic motion between WT and mutant was a little more than that of the apo protein relative to the motion of residues in the dimer interface (Trp6 and Arg8), flap elbow (Pro39-Trp42), and fulcrum (Gly16-17) regions. However, as expected, the difference in the dynamic motion of the flap tip region is smaller due to the binding of the inhibitor. For both the apo and complexed HIV-pr, the analysis indicates many intriguing effects due to the double mutant, I50L/A71V. The flap curling and opening events in I50L/A71V-HIV-pr are more stable than those in the WT and I50V mutant. The average flap

tip-active site, flap-flap distances, and curling behavior of the TriCa angles suggests a closer movement of flaps in the double mutant as compared to WT and I50V, probably making the active site volume smaller. The reduced active site conformations of the double mutant due to the flap dynamics behavior may enhance the binding of the inhibitor to the active site region. This may be due to the decreased flexibility in the active site leading to the decrease in K_m , i.e., an increase in the affinity of the enzyme for the inhibitor and stronger binding.⁴⁹ The most distinct motion for the HIV-pr complex was the movement of the side chain of catalytic Asp25 about the inhibitor. There is a flip-flop of the interaction between the catalytic Asp25 OD1/OD2 atoms and O18 of TMC114. This may be due to the effect of the mutation A71V from the double mutant, where the change from Ala71 to Val modifies the H-bonding pattern between the four antiparallel β -sheets connecting the Asp25 site to Val71. The change in the H-bonding pattern induces the rearrangement of β -sheets and finally affects the dynamics of Asp25 residues. The flip-flop interactions justify that the inhibitor tries to bind to either of the OD1/OD2 atoms of Asp25 in I50L/A71V, which seems to be different from that of WT and I50V. Consequently, the binding of the inhibitor to the protein differs for the double mutant. Such finding suggests a replacement of a different group at the O18 atom of TMC114 might provide the better binding properties.

In line with the previous studies, as compared with the WT-HIV-pr, the decrease of the binding affinity of I50V-HIV-pr to TMC114 was confirmed. The decrease in the binding affinity derives the drug resistance, which was experimentally discovered by Kovalevsky et al.⁴ However, the double mutant I50L/A71V-HIV-pr displays an enhanced binding to the inhibitor relative to the WT-HIV-pr. The increase of the binding implies that the double mutant I50L/A71V may be well adapted by the TMC114. The energy decomposition analysis suggests that the increase of the binding affinity for the double mutant I50L/A71V can be mainly attributed to the increase in electrostatic and van der Waals energies, which are canceled out in part by the increase of polar solvation energy. A per-residue basis decomposition investigation shows that the I50L/A71V mutant directly increases the binding affinity by approximately -0.88 (Ile50 to Leu50) and -0.90 (Ile50' to Leu50') kcal/mol, accounting for 45% of the total gain of the binding affinity. Besides the direct effect from the residues Leu50 and Leu50', the residue Gly49' considerably increases the binding affinity of

I50L/A71V–HIV-pr to the inhibitor by -0.74 kcal/mol to which the electrostatic interaction of Leu50's backbone contributes by -1.23 kcal/mol. Another two residues, Ile84 and Ile47', also increase the binding affinity by -0.22 and -0.29 kcal/mol, respectively, which can be mainly attributed to van der Waals terms (ΔT_{vdw} , -0.21 and -0.39 kcal/mol).

5. CONCLUSIONS

The double mutant I50L/A71V HIV-pr exhibits different conformation and dynamic behavior to the TMC114 inhibitor, e.g., closer movement of flaps, and flip-flop interaction between the catalytic Asp25 OD1/OD2 atoms and O18 of TMC114, which may imply less drug resistance, which was further verified in terms of binding affinity to the inhibitor in the energetic calculation. On the basis of the structural energetic analysis, we can conclude that the direct effects by the decrease in van der Waals energies for residues Val50 and Val50' and the increase in polar solvation energy for Val50' mainly accomplish the drug resistance in the I50V mutant. However, for the double mutant I50L/A71V, the increase in the binding affinity can be mainly attributed to the increase in electrostatic and van der Waals energies of residues Leu50 and Leu50' with considerable aid from the other flap residues Gly49', Ile47', and active site residue Ile84. As for the other protease inhibitors, the increase of the binding affinity implies that the double mutant I50L/A71V may be well adapted by the TMC114. The present article offers a quantitative and mechanistic rationalization of mutational effect from a comprehensive analysis of the structure–affinity relationship. We anticipate that, the current study can give some useful insights into the nature of mutational effect, and the difference in binding affinity for darunavir in protease variants may support the future design of more potent and effective HIV-pr inhibitors.

■ ASSOCIATED CONTENT

Supporting Information

Figure S1 displays root-mean-square displacement (rmsd) plot for backbone $C\alpha$ atoms relative to their initial minimized apo structures as a function of time. Table S1 summarizes the binding affinities from two parallel simulations. This material is available free of charge via the Internet at <http://pubs.acs.org>.

■ AUTHOR INFORMATION

Corresponding Author

*E-mail: yixuan.wang@asurams.edu.

Notes

The authors declare no competing financial interest.

■ ACKNOWLEDGMENTS

This work was supported by the National Institute of General Medical of the National Institute of Health (SC3GM082324 and 2R25GM071415), the American Recovery and Reinvestment Act (3SC3GM082324-02S1), and ACS PRF (47286-GB5) in terms of scholarly development. We thank Pittsburgh Supercomputing Center, NCSA-Teragrid, for providing the computational facilities to carry out the work in the form of a start-up grant (CHE100117).

■ REFERENCES

- Wlodawer, A.; Vondrasek, J. *Annu. Rev. Biophys. Biomol. Struct.* 1998, 27, 249–284.
- Wu, T. D.; Schiffer, C. A.; Gonzales, M. J.; Taylor, J.; Kantor, R.; Chou, S.; Israelski, D.; Zolopa, A. R.; Fessel, W. J.; Shafer, R. W. *J. Virol.* 2003, 77, 4836–4847.
- Tie, Y.; Boross, P. I.; Wang, Y.-F.; Gaddis, L.; Hussain, A. K.; Leshchenko, S.; Ghosh, A. K.; Louis, J. M.; Harrison, R. W.; Weber, I. T. *J. Mol. Biol.* 2004, 338, 341–352.
- Kovalevsky, A. Y.; Tie, Y.; Liu, F.; Boross, P. I.; Wang, Y.-F.; Leshchenko, S.; Ghosh, A. K.; Harrison, R. W.; Weber, I. T. *J. Med. Chem.* 2006, 49, 1379–1387.
- Wang, Y. F.; Tie, Y.; Boross, P. I.; Tozser, J.; Ghosh, A. K.; Harrison, R. W.; Weber, I. T. *J. Med. Chem.* 2007, 50, 4509–4515.
- Chen, J.; Zhang, S.; Liu, X.; Zhang, Q. *J. Mol. Model.* 2010, 16, 459–468.
- Hu, G. D.; Zhu, T.; Zhang, S. L.; Wang, D.; Zhang, Q. *G. Eur. J. Med. Chem.* 2010, 45, 227–235.
- Cai, Y.; Schiffer, C. A. *J. Chem. Theory Comput.* 2010, 6, 1358–1368.
- Stoica, I.; Sadiq, S. K.; Coveney, P. V. *J. Am. Chem. Soc.* 2008, 130, 2639–2648.
- Hou, T.; Yu, R. *J. Med. Chem.* 2007, 50, 1177–1188.
- Ode, H.; Neya, S.; Hata, M.; Sugiura, W.; Hoshino, T. *J. Am. Chem. Soc.* 2006, 128, 7887–7895.
- Ode, H.; Matsuyama, S.; Hata, M.; Hoshino, T.; Kakizawa, J.; Sugiura, W. *J. Med. Chem.* 2007, 50, 1768–1777.
- Wang, W.; Kollman, P. A. *Proc. Natl. Acad. Sci. U.S.A.* 2001, 98, 14937–14942.
- Yanchunas, J. Jr.; Langley, D. R.; Tao, L.; Rose, R. E.; Friberg, J.; Colonna, R. J.; Doyle, M. L. *Antimicrob. Agents Chemother.* 2005, 49, 3825–3832.
- Colonna, R.; Rose, R.; McLaren, C.; Thiry, A.; Parkin, N.; Friberg, J. *J. Infect. Dis.* 2004, 189, 1802–1810.
- Skalova, T.; Dohnalek, J.; Duskova, J.; Petrokova, H.; Hradilek, M.; Soucek, M.; Konvalinka, J.; Hasek, J. *J. Med. Chem.* 2006, 49, 5777–5784.
- Weinheimer, S.; Discotto, L.; Friberg, J.; Yang, H.; Colonna, R. *Antimicrob. Agents Chemother.* 2005, 49, 3816–3824.
- Wu, E. L.; Han, K.; Zhang, J. *Z. Chemistry* 2008, 14, 8704–8714.
- Hou, T.; Zhang, W.; Case, D. A.; Wang, W. *J. Mol. Biol.* 2008, 376, 1201–1214.
- Wu, E. L.; Mei, Y.; Han, K.; Zhang, J. *Z. Biophys. J.* 2007, 92, 4244–4253.
- Xu, Y.; Wang, R. *Proteins* 2006, 64, 1058–1068.
- Strockbine, B.; Rizzo, R. C. *Proteins* 2007, 67, 630–642.
- Zou, H.; Luo, C.; Zheng, S.; Luo, X.; Zhu, W.; Chen, K.; Shen, J.; Jiang, H. *J. Phys. Chem. B* 2007, 111, 9104–9113.
- Wang, J.; Morin, P.; Wang, W.; Kollman, P. A. *J. Am. Chem. Soc.* 2001, 123, 5221–5230.
- Cheatham, T. E. III; Srinivasan, J.; Case, D. A.; Kollman, P. A. *J. Biomol. Struct. Dyn.* 1998, 16, 265–280.
- Gohlke, H.; Kiel, C.; Case, D. A. *J. Mol. Biol.* 2003, 330, 891–913.
- Surleraux, D. L.; Tahri, A.; Verschueren, W. G.; Pille, G. M.; de Kock, H. A.; Jonckers, T. H.; Peeters, A.; De Meyer, S.; Azijn, H.; Pauwels, R.; et al. *J. Med. Chem.* 2005, 48, 1813–1822.
- Prabu-Jeyabalan, M.; Ng, C.; King, N. M.; Bandaranayake, R.; Naliveika, E. A.; Schiffer, C. A. RSCB-PDB; DOI:10.2210/pdb3me3/pdb.
- Hyland, L. J.; Tomaszek, T. A. Jr.; Meek, T. D. *Biochemistry* 1991, 30, 8454–8463.
- Wang, Y. X.; Freedberg, D. I.; Yamazaki, T.; Wingfield, P. T.; Stahl, S. J.; Kaufman, J. D.; Kiso, Y.; Torchia, D. A. *Biochemistry* 1996, 35, 9945–9950.
- Bayly, C. I.; Cieplak, P.; Cornell, W.; Kollman, P. A. *J. Phys. Chem.* 1993, 97, 10269–10280.
- Dewar, M. J. S.; Zoebisch, E. G.; Healy, E. F.; Stewart, J. J. P. *J. Am. Chem. Soc.* 1985, 107, 3902–3909.
- Wang, J.; Wolf, R. M.; Caldwell, J. W.; Kollman, P. A.; Case, D. A. *J. Comput. Chem.* 2004, 25, 1157–1174.

- (34) Case, D. A.; Darden, T. A.; Cheatham, T. E., III; Simmerling, C. L.; Wang, J.; Duke, R. E.; Luo, R.; Crowley, M.; Walker, R. C.; Zhang, W.; et al. *AMBER 10*; University of California: San Francisco, CA, 2008.
- (35) Hornak, V.; Abel, R.; Okur, A.; Strockbine, B.; Roitberg, A.; Simmerling, C. *Proteins* **2006**, *65*, 712–725.
- (36) Jorgensen, W. L.; Chandrasekhar, J.; Madura, J. D.; Impey, R. W.; Klein, M. L. *J. Chem. Phys.* **1983**, *79*, 926–935.
- (37) Essmann, U.; Perera, L.; Berkowitz, M. L.; Darden, T.; Lee, H.; Pedersen, L. G. *J. Chem. Phys.* **1995**, *103*, 8577–8593.
- (38) Berendsen, H. J. C.; Postma, J. P. M.; Van Gunsteren, W. F.; DiNola, A.; Haak, J. R. *J. Chem. Phys.* **1984**, *81*, 3684–3693.
- (39) Ryckaert, J.-P.; Ciccotti, G.; Berendsen, H. J. C. *J. Comput. Phys.* **1977**, *23*, 327–341.
- (40) Onufriev, A.; Bashford, D.; Case, D. A. *J. Phys. Chem. B* **2000**, *104*, 3712–3720.
- (41) Schrödinger, LLC. *PyMol*, version 1.3. www.pymol.org
- (42) Todd, M. J.; Freire, E. *Proteins: Struct., Funct., Genet.* **1999**, *36*, 147–156.
- (43) Maschera, B.; Darby, G.; Palu, G.; Wright, L. L.; Tisdale, M.; Myers, R.; Blair, E. D.; Furfine, E. S. *J. Biol. Chem.* **1996**, *271*, 33231–33235.
- (44) Perryman, A. L.; Lin, J. H.; McCammon, J. A. *Protein Sci.* **2004**, *13*, 1108–1123.
- (45) Piana, S.; Carloni, P.; Rothlisberger, U. *Protein Sci.* **2002**, *11*, 2393–2402.
- (46) Scott, W. R.; Schiffer, C. A. *Structure* **2000**, *8*, 1259–1265.
- (47) Rick, S. W.; Erickson, J. W.; Burt, S. K. *Proteins* **1998**, *32*, 7–16.
- (48) Zhu, Z.; Schuster, D. I.; Tuckerman, M. E. *Biochemistry* **2003**, *42*, 1326–1333.
- (49) Zoldak, G.; Sprinzl, M.; Sedla, E. *Eur. J. Biochem.* **2004**, *271*, 48–57.
- (50) Freedberg, D. I.; Wang, Y. X.; Stahl, S. J.; Kaufman, J. D.; Wingfield, P. T.; Kiso, Y.; Torchia, D. A. *J. Am. Chem. Soc.* **1998**, *120*, 7916–7923.
- (51) Zoete, V.; Michelin, O.; Karplus, M. *J. Mol. Biol.* **2002**, *315*, 21–52.
- (52) Ishima, R.; Freedberg, D. I.; Wang, Y. X.; Louis, J. M.; Torchia, D. A. *Structure* **1999**, *7*, 1047–1055.
- (53) Bandyopadhyay, P.; Meher, B. R. *Chem. Biol. Drug Des.* **2006**, *67*, 155–161.
- (54) Nalam, M. N.; Ali, A.; Altman, M. D.; Reddy, G. S.; Chellappan, S.; Kairys, V.; Ozen, A.; Cao, H.; Gilson, M. K.; Tidor, B.; Rana, T. M.; Schiffer, C. A. *J. Virol.* **2010**, *84*, 5368–5378.
- (55) King, N. M.; Prabu-Jeyabalan, M.; Nalivaika, E. A.; Wigerinck, P.; Béthune, M.-P. D.; Schiffer, C. A. *J. Virol.* **2004**, *78*, 12012–12021.